PLASMODIUM EXOERYTHROCYTIC PARASITES REDIRECT TRAFFICKING OF HUMAN PROTEINS TO THE PARASITOPHOROUS VACUOLE

Jaeson Calla[1], Nimisha Mittal[1], Greg LaMonte[1], Benjamin Liffner[2], Karla P. Godinez-Macias[1], Krypton Carolino[1], Gregory T. Walker[1], Bing Yu Zou[1], Emma Paytas[1], Layné Guerra[3], Carlos Tong-Rios[3], Brice Campo[4], Joseph M. Vinetz[3,5], Dionicia Gamboa[3], Manuela Raffatellu[1,6,7], Sabrina Absalon[2], and Elizabeth A. Winzeler[1]

Affiliations:

[1]Department of Pediatrics, Division of Host-Microbe Systems & Therapeutics, School of Medicine, University of California, San Diego, La Jolla, United States of America.

[2]Department of Pharmacology and Toxicology, Indiana University School of Medicine, Indianapolis, United States of America.

[3]Laboratorio ICEMR-Amazonia, Laboratorios de Investigación y Desarrollo, Facultad de Ciencias y Filosofía, Universidad Peruana Cayetano Heredia, Lima, Peru.

[4]Medicines for Malaria Venture, Geneva, Switzerland.

[5]Current address: Department of Internal Medicine, Section of Infectious Diseases, School of Medicine, Yale University, New Haven, United States of America.

[6]Center for Microbiome Innovation, University of California San Diego, La Jolla, United States of America.

[7]Chiba University-UC San Diego Center for Mucosal Immunology, Allergy, and Vaccines (CU-UCSD cMAV), La Jolla, United States of America.

To whom correspondence should be addressed: ewinzeler@health.ucsd.edu (EW)

KEYWORDS

Hypnozoite, malaria, *P. vivax*, Hepatocyte.

ABBREVIATIONS USED

PVR, Parasitophorous Vacuole Region; NR4A3, Nuclear receptor subfamily 4 group A member 3, HCI, High Content Imaging; qRT-PCR quantitative Reverse Transcriptase Polymerase Chain Reaction; ATQ, Atovaquone; EEF, Exoerythrocytic form; FC, flow cytometry; FACS, Fluorescence-Activated Cell Sorting; hpi, hours post infection; TRAP, Thrombospondin Related Anonymous Protein; GOLGA8A, Golgin subfamily A member 8A; MUC13, Mucin 13; CGA, Glycoprotein hormones alpha chain; Binding immunoglobulin protein, BiP; CXCL2, Chemokine

35 (C-X-C Motif) Ligand 2; CSP, Circumsporozoite protein; UIS4, Up-regulated in infective
36 sporozoites gene 4; Lipopolysaccharide, LPS.

ABSTRACT

Changes in host cell morphology and transcription after apicomplexan parasite infection have long been noted, but there have been few studies of the functional consequences of host cell remodeling. Here we show, using time-dependent immunofluorescence microscopy of multiple human cell lines (HepG2, HC-04, Huh7.5.1 and primary human hepatocytes), infected with multiple *Plasmodium* species (*Plasmodium berghei, P. falciparum* and *P. vivax* (hypnozoites and schizonts)), and antibodies to multiple human proteins (HsNR4A3, HsMUC13, HsGOLGA8A, HsCGA, HsBiP, HsCXCL2), that human protein trafficking is extensively modified in *Plasmodium* infected cells. Using conventional as well as ultrastructure expansion microscopy we show that newly-synthesized human proteins are trafficked to the parasitophorous vacuole instead of the infected-cell plasma membrane, nucleus or extracellular space. Universal redirection of human signaling proteins cells the parasitophorous vacuole may provide a mechanistic explanation for how apicomplexan parasites can block host cells response to infection.

INTRODUCTION

Malaria remains a worldwide problem with up to 241 million cases reported in 2021[1]. Given the economic and humanitarian burden of malaria, and the continual emergence of parasite resistance to drugs that act against the symptomatic stages of the infection, new strategies to treat, prevent or control malaria are needed.

Liver cells are the primary cellular target of the *Plasmodium* parasite's exoerythrocytic stage. After injection into the vertebrate host by the bite of an infected Anopheline mosquito, the parasites (sporozoites) travel to the liver where they migrate and cross through several barriers. These barriers include endothelial cells, dermal fibroblast, liver sinusoidal endothelial cells (LSECs) and highly phagocytic Kupffer cells, that allows sporozoites to pass all barriers to find and infect hepatocytes[2,3]. When a suitable hepatocyte is reached, they inject the contents of their apical organelles using their specialized secretory organelles, the micronemes and rhoptries, into the hepatocyte membrane creating a molecular machine that enables the formation of a vacuole in the host cell cytoplasm[4]. The vacuole will enclose and protect the parasite and is surrounded by a host-derived parasitophorous vacuole membrane (PVM)[5]. Similar vacuoles are formed when

65 blood stage malaria parasites invade erythrocytes and by other apicomplexan parasites, including
66 *Toxoplasma gondii* when they invade fibroblasts, for example[6]. Some malaria parasite species can
67 also remain in the liver in a dormant state, called a hypnozoite[7]. Hypnozoite-forming species,
68 especially *P. vivax*, represent barriers to malaria eradication because if they are not eliminated by
69 drug treatment, they can reawake months to years later, leading to patient relapse, as well as active
70 malaria transmission in an area that was once cleared of malaria. Despite their importance,
71 hypnozoites are poorly understood.

72 There are no clinical symptoms associated with liver stage infection[8]. Fever and chills that
73 are characteristic of malaria only develop after the merozoites are released from the schizont and
74 move to the circulatory system scanning for their next target cells, the erythrocytes.

75 Pre-erythrocytic stages are the primary target for the development of malaria vaccines. It
76 has been suggested that vaccines directed at this stage will be more effective because they will
77 suppress the spread of vaccine-resistance because of low parasite numbers at this stage (hundreds
78 versus billions in blood stages) and the only licensed vaccine, RTS, S/AS01, Mosquirix™, consists
79 of a target, circumsporozoite protein (CSP), which is highly expressed in *Plasmodium*
80 sporozoites[9-11]. Irradiated sporozoites also provide strong protection against malaria and have been
81 used in vaccine trials[12-14]. Irradiated sporozoites invade hepatocytes, form a trophozoite, but then
82 the host cell will apoptose before merozoite maturation is complete, allowing the display of
83 antigens and potentially elicit an improved immune response that is missing with unirradiated
84 sporozoites[15]. Vaccination with parasites that have mutations in PV-localized UIS3 and UIS4
85 result in an unprotective infection and sterile protection against challenge[16].

86 In the course of their development, erythrocytes will have shed many of their organelles,
87 including their nuclei, before they become susceptible to invasion by malaria parasites.
88 Hepatocytes, on the other hand, have nuclei and remain transcriptionally active after parasite
89 invasion. We had previously performed a dual RNAseq study on flow-sorted, *P. berghei*-infected
90 liver cells[17]. The experiments, which were conducted in a variety of time points and on different
91 cell types showed concerted patterns of gene upregulation, including genes involved in the immune
92 response, such as the mucin, *HsMUC13*[17]. Curiously, we observed that HsMUC13 protein
93 colocalized with parasite UIS4, a protein inserted into the PVM in infected cells[17]. To further

94 investigate these phenomena, here we examine other human genes that were upregulated after
95 parasite infection, including the orphan human nuclear hormone receptor, *HsNR4A3*.

96 Surprisingly, we find that the cognate protein for all upregulated human genes that we
97 examine show colocalization with the parasite parasitophorous vacuole (PV) marker, UIS4[18]. We
98 show this colocalization is observed not only for *P. berghei* and *P. falciparum* liver stages, but for
99 both *P. vivax* schizonts and hypnozoites as well. Furthermore, using ultrastructure expansion
100 microscopy, a recently developed sample preparation method that enabled the isotropic expansion
101 of *Plasmodium* parasites up to 4.5-fold[19], we revealed the association of HsNR4A3 proteins with
102 the PVM of *P. berghei* parasite. Our data indicate that in all these parasites, host proteins are being
103 redirected to the PV. We propose that apicomplexan parasites manipulate host secretion apparatus
104 to favor their development and to hide from the immune system.

105 RESULTS

106 *Host proteins are transcriptionally upregulated during P. berghei infection of liver cells*

107 A previous dual (parasite and human) RNA-seq study with the rodent malaria parasite, *P.*
108 *berghei* (*Pb*GFP-SM_{CON} (*Pb*-GFP)), identified a series of human transcripts that were upregulated
109 during parasite exoerythrocytic infection (Fig. 1a, 1b). Multiple time points, replicates, and
110 different hepatoma host cells (HepG2s, Huh7.5.1s, HC-04s) were used in these experiments in
111 which human cells were individually sorted into infected and noninfected pools based on the
112 presence of parasite-encoded GFP signal. Oddly, the most upregulated and statistically significant
113 genes across cell lines at 48 hours did not seem to be functionally related to one another. *HsMUC13*
114 encodes a secreted membrane localized mucin that is usually expressed in the gut. It is normally
115 upregulated after infection and is asymmetrically localized to luminal side of gut epithelial cells[20].
116 We had previously shown that it colocalized to the parasite vacuole in mature *P. vivax* and *P.*
117 *berghei* schizonts[17]. Also upregulated in multiple hepatocyte-derived lines was *HsNR4A3* ($p =$
118 2.8×10^{-30}). The NR4A subfamily encodes orphan nuclear receptors that belong to the larger nuclear
119 receptors (NRs) superfamily of eukaryotic transcription factors. The NR4A subfamily includes
120 three members, namely NUR77 (HsNR4A1), NURR1 (HsNR4A2) and NOR1 (HsNR4A3), which
121 are gene regulators and participate in diverse biological functions. Although exact function of

122 HsNR4A3 is not known, data suggest a potential role in controlling glucose in some cell types[21].
123 NR4A3 knockout mice show expansion of the pancreatic beta cells, needed for insulin production,
124 and NR4A3 overexpression lines increase glucose production in response to some stimuli, and act
125 as activator of beta cell proliferation and insulin production[22,23]. It has also been reported as an
126 NLRP3 inflammasome activation-responsive gene[24]. In the cancer arena, it has been shown that
127 NR4A3 overexpression attenuates proliferation of cancer cells and promotes apoptosis by
128 augmenting the expression of pro-apoptotic genes via a p53 dependent mechanism[25]. *HsCGA*
129 (adjusted $p = 4.4\text{x}10^{-13}$) encodes the shared alpha chain of the heterodimeric human glycoprotein
130 hormones; thyrotropin/thyroid stimulating hormone/TSH, lutropin/luteinizing hormone/LH,
131 follitropin/follicle stimulating hormone/FSH and choriogonadotropin/CG. HsCGA, along with its
132 partner, would normally be secreted into the bloodstream where it would bind rhodopsin-like G
133 protein-coupled receptors on the target cell[26]. *HsCGA* is expressed at high levels in the placenta
134 but is also upregulated in breast cancer and is an estrogen receptor alpha (ERα)-responsive gene
135 in human breast tumors[27]. *HsTAS2R4* encodes a G-protein coupled receptor that is normally
136 expressed on the surface of tongue epithelial cells. It is responsive to bitter molecules, including,
137 interestingly, the antimalarial, quinine but may also play a role in small molecule-sensing in
138 extraoral cell types[28].

139 In addition, the set of statistically significant upregulated genes included several noncoding
140 genes. The lncRNA, *HsNEAT1* (adjusted $p = 1.8\text{x}10^{-34}$), promotes activation of inflammasomes in
141 macrophages[29]. *HsMALAT1*, also known as *HsNEAT2* is also a large, non-coding RNA, which is
142 highly conserved amongst mammals and highly expressed. Overexpression of *HsMALAT1*
143 suppresses breast cancer metastasis in transgenic, xenograft, and syngeneic models of cancer[30] and
144 is also strongly associated with inflammasome activation[31].

145 Because the RNAseq studies had been performed on model hepatoma cells lines we used
146 qRT-PCR to confirm the upregulation of *HsNR4A3, HsMUC13, HsCGA, HsSLC22A8,*
147 *HsMALAT1, HsRASSSF9, HsSDHA, HsSLC25A27, HsNEAT1,* and *HsTAS2R4* in *P. berghei*-
148 infected primary human hepatocytes, as well as in *P. berghei* infected Huh7.5.1, HepG2 and HC-
149 04 cells. Cells were infected with *P. berghei* expressing GFP and flow sorted. RNA was extracted
150 from infected cells, as well as from control, parallel non-infected cells. In these four cell lines, we
151 observed consistent 13-20-fold upregulation of *HsNR4A3* in all cell lines except for HepG2 cells

152 (Fig. 1c). We also observed upregulation of other transcripts via qRT-PCRs but not as consistently
153 across all lines.

154 To further ensure that the patterns were not specific to parasites, we performed Western
155 blot analysis. We obtained several commercial antibodies to some of the different human proteins
156 that showed the highest, most significant, and reproducible upregulation. These included
157 HsNR4A3, HsCGA, and HsMUC13. HsGOLGA8A, was also included (probability of
158 upregulation of chance = 4.04×10^{-10}). It encodes a member of the Golgin family of membrane
159 proteins which play a role in tethering vesicles to the Golgi apparatus[32],[33]. All 21 annotated Golgins
160 were amongst the set of upregulated genes in infected cells, 13 significantly (hypergeometric mean
161 probability of enrichment by chance = 5.5×10^{-5}), with an average upregulation of 2.3×. The bulk
162 cultures as well as uninfected HC04 control cultures were infected with both *P. berghei* and *P.*
163 *falciparum*. All the evaluated antibodies showed recognition of a single band corresponding to the
164 native protein (Fig. S1a, S1b). In some cases, upregulation was observed relative to human control
165 protein (Hs-Vinculin, Fig. S1b), but given that only a small proportion of cells are infected in bulk
166 cultures (1 to 2%), especially with *P. falciparum*, we did not attempt to further quantify this. The
167 antibody to CGA1 recognized a larger than expected protein. CGA1 is heavily glycosylated which
168 may contribute to the size difference.

169 *Upregulated host proteins show colocalization with PVM via immunofluorescence analysis.*

170 Given the challenges of analyzing level by Western we next used immunofluorescence and
171 confocal microscopy to confirm our RNA-seq results. First, assays were performed with mature
172 *P. berghei*, the species on which hepatocyte flow sorting was performed. Isolated *P. berghei*
173 sporozoites were incubated with a permissive human liver cell line, HC-04. After 48 hours, the
174 cultures were fixed and stained with a set of primary commercial antibodies against various
175 upregulated hepatocyte proteins (HsNR4A3, HsCGA, HsGOLGA8A, and HsMUC13), and to
176 parasite UIS4 (Fig. 2a), a parasite protein highly expressed in sporozoites and liver stages of
177 multiple *Plasmodium* species, and which localizes to the PVM in both hypnozoites and schizonts[34].
178 All antibodies (against HsNR4A3, HsCGA, HsGOLGA8A, and HsMUC13 proteins) showed high
179 expression of their cognate proteins in *P. berghei*-infected but not -uninfected HC-04 cells.
180 Interestingly, all four host proteins colocalized with the parasite marker, UIS4 (Fig. 2a). HsNR4A3

181 is normally localized to the nucleus[35] and indeed staining was observed in the nucleus in uninfected
182 cells visible in the image. A zoom in (Fig. 2a1), a panoramic view (Fig. 2a2), and a panoramic
183 overexposed view (Fig. 2a3) is also shown for the HsNR4A3 protein. GOLGA8A encodes protein
184 with an N-terminal coiled-coil domain and a single C-terminal transmembrane domain and is also
185 known as golgin-67. It localized to the Golgi apparatus which in most human cells is adjacent to
186 the nucleus[36]. As expected, our staining showed weak HsGOLGA8A surrounding the nucleus in
187 uninfected cells. MUC13 and CGA are both expected to be secreted into the extracellular space.
188 Uninfected cells showed some weak diffuse cytoplasmic staining with antibodies to these proteins.

189 To determine if similar staining would be observed in human cells infected with the human
190 pathogen, *P. falciparum,* we performed experiments using dissected *P. falciparum* sporozoites and
191 primary hepatocytes. Sporozoites were placed on primary hepatocytes in 96-well plates and
192 cultures were incubated for 120 hours, necessary because of the longer *P. falciparum* liver
193 development time. Immunofluorescence was performed using a *P. vivax* antibody to PvUIS4[34]
194 (which is cross-reactive with PbUIS4, and PfUIS4) (Fig. 2b) and anti-human primary antibodies.
195 These experiments confirmed upregulation of the HsNR4A3, HsCGA, HsGOLGA8A, and
196 HsMUC13 proteins with staining, as with *P. berghei*, occurring in the PVM region, overlapping
197 largely with UIS4 staining. Importantly, these data showed that the staining patterns were not
198 associated with the use of a hepatoma cell line and were conserved in primary human hepatocytes.

199 We next examined another human pathogen, *P. vivax,* which can remain in an infected
200 liver cell as a hypnozoite that can be activated months or years after the primary infection. As *P.*
201 *vivax* cannot be maintained in cell culture, patients diagnosed with *P. vivax* malaria, were recruited,
202 and asked to provide 20mL of whole blood, which was used to feed fasted, female *Anopheles*
203 *darlingi* mosquitoes using a standard membrane feeding assay. After 14 days the mosquitoes were
204 dissected to obtain sporozoites, which were used to infect HC-04 cell lines (see Methods). After
205 five days, the cells were fixed and stained with our primary antibodies (against HsNR4A3,
206 HsCGA, HsGOLGA8A, and HsMUC13 proteins). Again, all antibodies showed strong
207 colocalization with the parasites (Fig. 2c) for all proteins.

208 To determine whether this pattern would be observed for hypnozoites we searched for UIS4
209 positive objects that were smaller than 10µm and which showed characteristic circular patterns

210 associated with UIS4 signal, the bonafide way to identify hypnozoites[34]. For our *P. vivax* infected
211 samples, we identified hypnozoites at a rate of 1 per 5,000 hepatocytes, and schizonts at a
212 frequency of ~1:1,000, some of which are shown in Fig. 2d. Interestingly, the same
213 immunofluorescent micrographs also showed colocalization with HsNR4A3, HsCGA,
214 HsGOLGA8A, and the HsMUC13 (Fig. 2d), a zoom-in for HsNR4A3 protein in hypnozoites
215 stages is shown (Fig. 2d1). In fact, previous parasite-associated immunolocalization had been
216 observed for HsMUC13[17]. Analysis of the images showed a strong correlation between UIS4 and
217 the different tested proteins for all species (Fig. S2).

218 While the relocalization of one protein could be functional, the relocalization of all was
219 puzzling. These micrographs showed similar localization of the human proteins, ruling out the
220 possibility of the species-specific secondary antibodies cross-reacting with the primary UIS4
221 antibody. In addition, we repeated IFAs with a variety of different primary antibodies using the *P.*
222 *berghei* infection model and in all cases, the same patterns were obtained (Fig. S3).

223 *HsNR4A3 edited lines show decreased NR4A3 staining in Westerns and IFA*

224 To further assess the question of antibody specificity as well as HsNR4A3 functionality,
225 we next performed knockouts on *HsNR4A3*. We used CRISPR/*Cas9*-based methods to disrupt
226 *HsNR4A3* in clonal HC-04 cell lines using two different approaches (two plasmid or single
227 plasmid) and different guide RNA sets (Fig. S4a and S4b), obtaining six different stably edited
228 clones (GL1, GL2, and GL3 and NM1, NM2, and NM3 created using the two approaches)).
229 Western blot analysis showed lower expression of HsNR4A3 in five of six clones (clones GL1 and
230 GL3 and NM1, NM2, and NM3)) relative to native HC-04 cells (Fig. S4c, S4d).

231 To evaluate antibody specificity, *HsNR4A3* knockout cells were infected with *P. berghei*
232 (*Pb*-ANKA-GFP-Luc SMCON (*Pb*-Luc)) sporozoites. After 48hpi, the infected and uninfected
233 cells were evaluated by immunofluorescence and confocal microscopy. For HC-04 HsNR4A3
234 unmodified cells (WT) we observed colocalization with the parasite markers UIS4 (Fig. S4e) and
235 HSP70 (Fig. S4e, S4f). In contrast, no NR4A3 staining was observed in *HsNR4A3* knockout cells
236 (Fig. S4e) and pattern quantification showed no correlation ($p < 0.0005$) Fig. S4f). Staining was
237 similar to the negative control in which the NR4A3 antibody was not used. These data largely rule

238 out the possibility of NR4A3 antibody cross-hybridization with an as-yet unspecified parasite
239 protein.

240 To confirm our findings in *P. vivax*, we also performed *in vitro* infection tests using cloned
241 GL1 and GL3 *HsNR4A3* knockout cells and *P. vivax* parasites obtained as described above. We
242 observed a marked expression of the HsNR4A3 protein in the HC-04 HsNR4A3 WT cells in the
243 two stages of the parasite (hypnozoites and schizonts) showing the expected co-staining with UIS4.
244 For clone GL1, we did not identify any parasites (see below) while for clone GL3 (Fig. S4g), we
245 observed no signal or co-staining with UIS4. A statistically-significant loss of staining correlation
246 in *HsNR4A3* knockouts was confirmed by image quantitation (Fig. S4h, S4i).

247 *Role of the protein HsNR4A3 in exoerythrocytic infections*

248 To determine whether HsNR4A3 contributes to parasite growth and development we
249 investigated both schizont size, schizont number and schizont morphology in the *HsNR4A3*
250 knockout clones in *P. berghei* and *P. vivax*. First, *in vitro* infections with *P. berghei* parasites were
251 carried out. We performed a qRT-PCR experiment using primers to the *P. berghei* 18S RNA gene
252 as previously described[37]. These data showed that a higher number of cycles were needed to detect
253 parasites in NM1, NM2 and NM3 clones, with NM3 requiring almost as many cycles for detection
254 as treatment with 5 nM atovaquone, a drug which completely blocks parasite exoerythrocytic
255 development (Fig. S5a). Next, high content imaging analysis was performed on *P. berghei* infected
256 cells and used to determine the number of UIS4 positive objects per field (0.8cm^2). These data
257 showed a ~70% reduction in the relative number of parasites in all three *HsNR4A3* knockout clones
258 (Fig. S5b). We also observe that most of the positive objects identified in *HsNR4A3* knockout cells
259 (NM1-NM3) have a diameter of 5 µm compared with 40µm the WT HC-04 cells (Fig. S5c).

260 To investigate the role of HsNR4A3 in *P. vivax* development, we infected our GL1 and
261 GL3 *HsNR4A3* knockout lines with *P vivax* sporozoites, obtained as described above, and allowed
262 the parasites to develop for 120 hours. Cultures were co-stained with the UIS4 parasite marker to
263 identify and count infected cells. Hypnozoites were distinguished from schizonts based on parasite
264 size (Fig. S5d, S5e). In both clones we observed fewer schizonts, although the reduction in the
265 number of hypnozoites was not as marked. This suggests that the expression of the HsNR4A3
266 protein is needed for the *P. vivax* parasite to complete the schizont maturation process. To

267 determine if this was true for *P. berghei* as well, we also infected the *HsNR4A3* knockout clones
268 with GFP-expressing *P. berghei* sporozoites and performed flow sorting of GFP-positive objects
269 on GL1 and WT HC-04 cells after 48 hours incubation (Fig. S5f). We observed a marked reduction
270 in the number of GFP positive objects in GL1. These data suggest that HsNR4A3-depleted HC-04
271 cells may be less able to support parasite invasion and maturation but also highlight that different
272 clones have different levels of gene disruption in diploid human cells, and the phenotype is slightly
273 inconsistent.

274 On the other hand, all experiments described above were normalized to the number of
275 human cells (at either the cell counting level or via total RNA in the qPCR studies) and if human
276 cells grew faster this would contribute to lower relative parasite numbers after a 48-hour incubation
277 and an even greater reduction with P. vivax infections. Because it has been reported that
278 HsNR4A3-edited human breast and lung cancer cells (MDA-MB-231 and H1299, respectively)
279 show increased cell proliferation[25], we measured growth rates in the NM1 and NM3 clones and
280 indeed observed 3 to 6 × more cells in comparison to the HC-04 HsNR4A3 WT cells 36 hours
281 after plating. Thus, although we do find that HsNR4A3 expression may help the parasites survive
282 and grow, the impact could be partially indirect.

283 *HsNR4A3 is trafficked to the parasitophorous vacuole membrane.*

284 As a nuclear hormone receptor, HsNR4A3 is expected to traffic between the nucleus and
285 cytoplasm. To study the temporal dynamics of HsNR4A3 relocalization in the context of a parasite
286 infection we next conducted a time course experiment in *P. berghei,* monitoring subcellular
287 localization of HsNR4A3 during exoerythrocytic infections. *P. berghei* sporozoites were placed
288 on HC-04 cells and samples were collected and fixed for immunofluorescence analysis every three
289 hours. At three hours, HsNR4A3 staining was observed in the host cell nucleus, overlapping with
290 host cell DAPI for both infected and uninfected cells, as expected for a nuclear hormone orphan
291 receptor, which are constitutively-active transcription factors (Fig. 3). In contrast, the parasite-
292 specific marker, UIS4, was clearly in the host cell cytoplasm, surrounding the parasite and only
293 found in infected cells. At later time points, HsNR4A3 was no longer found in the host nucleus,
294 and was now found in the cytoplasm of infected cells. By 12 hours, weak HsNR4A3 staining was
295 observed in the nucleus of uninfected cells, but strong staining was observed in infected cells in

296 the PVR. In late stages (24-72 hours), HsNR4A3 expression overlapped with the parasite marker,
297 UIS4 (Fig. 3a, 3b). Given the clear upregulation in NR4A3 gene expression in infected cells, these
298 patterns are consistent with newly synthesized NR4A3 being trafficked directly into the PVR
299 instead of to the host nucleus. Image quantification (Fig. S6a) showed little PbUIS4:HsNR4A3
300 correlation at early times (<0.1 at 3 hours) but strong correlation at later times (>0.9 at 96 hours),
301 and an inverse relationship with DAPI:HsNR4A3 correlation (Fig. S6b). Similar relocalization
302 patterns were also observed over the course of *P. berghei* exoerythrocytic development for
303 HsGOLGA8A (Fig. S7a, S7b) with the staining observed around the HC-04 cell nucleus at time
304 zero and then moving to co-localize with PbUIS4 by 48 hours in infected cells only. As a control,
305 we examined a gene that did not show differential regulation after infection. HsBiP, also known
306 as HsHSPA5 or GRP-78 is a highly expressed heat shock protein that is typically found in the
307 lumen of the ER and is a well-established marker of ER. It shows little evidence of differential
308 regulation after infection in our dual RNAseq study ($p = 0.97$, log2fold change = -0.006) but is
309 one of the most abundant transcripts (ranking at 96 of ~25,000 transcripts in terms of base mean
310 expression). Although in early stages of development it surrounded the host nuclei (Fig. S7c) as
311 predicted in all eukaryotic cells, it completely colocalized with PbUIS4 by 72 hours of infection
312 and image analysis showed strong correlation with PbUIS4 (Fig. S7d).

313 *Expansion immunofluorescence confocal microscopy localizes hsNR4A3 to the parasitophorous*
314 *vacuole.*

315 To further characterize the interaction of HsNR4A3 with the PVM we turned into
316 ultrastructure expansion microscopy (U-ExM) coupled with Airyscan super-resolution
317 microscopy[19,38]. We fixed and expanded Huh7.5.1. cells after 48 hours of infection with *P. berghei*
318 parasites. Previous work in blood-stage parasites demonstrated that the higher resolution achieved
319 post-expansion allows to distinguish the PVM from the parasite plasma membrane both stained by
320 Bodipy-TR-ceramide dye[38]. Using anti-UIS4 antibody in combination with Bodipy-TR ceramide
321 staining we expectedly localized UIS4 at the PVM and observed numerous UIS4-positive lipid-
322 enriched vesicles within the PV space or in the host-cytoplasm (Fig. S8). After the validation of
323 UIS4 as U-EXM compatible PVM marker, we used primary antibodies against HsNR4A3 and
324 UIS4 proteins and confirmed the close association of HsNR4A3 with the PVM. HsNR4A3
325 localized at the host-cytosolic side of the PVM in foci that predominantly are uniformly distributed

326 around the PV and occasionally concentrated in pockets associated with the PVM with some
327 staining in the PV (Fig. 4a).

328

329 *Secreted immune signaling molecules are also redirected to the PVR*

330 One unifying hypothesis that could explain the colocalization that was observed with many
331 of our examined proteins would be if all newly synthesized inter and intracellular host signaling
332 molecules were redirected away from their usual cytoplasmic or cell membrane location and into
333 the parasite vacuole membrane region PVM, potentially as a way to avoid immune signaling or
334 instructions to undergo apoptosis. To further investigate this, we examined the list of upregulated
335 genes to identify well-characterized cytokines and selected HsCXCL2 (Fig S9a, S9b), which was
336 expressed and upregulated in infected HC-04 cells in particular ($\log_2$ fold change = 2.76, p =
337 1.46×10^{-07}). *HsCXCL2* encodes a chemokine ligand that is secreted by monocytes and
338 macrophages at the site of inflammation and is strongly responsive to LPS stimulation. It binds to
339 the chemokine receptor, HsCXCR2 and plays a role in early stage of neutrophil recruitment during
340 tissue inflammation[39]. To test the hypothesis that HsCXCL2 would migrate to the PVR after
341 immune stimulation HC-04 cells were first infected with *P. berghei* and then after 24 hours treated
342 with LPS. Immunofluorescence assays using a CXCL2 antibody were performed at 2, 24 and 48
343 hours (26, 48 and 72hpi). These data showed a strong upregulation of CXCL2 expression in LPS-
344 treated, infected and uninfected HC-04 cells. As with other host proteins, HsCXCL2 staining
345 colocalized with the PVR and PbUIS4 in the infected cells (Fig. 5a, 5b). The specificity of
346 commercial antibodies against HsCXL2, HsBiP (Fig. S10a – Fig. S10d) and the controls (Fig.
347 S10e – Fig. S10f) are showed.

348 **DISCUSSION**

349 Here we have shown that five different upregulated proteins (HsNR4A3, HsCGA,
350 HsGOLGA8A, HsMUC13, and HsCXCL2), each with different, intracellular trafficking patterns,
351 all end up in the PV or PVR, surrounding the parasite. In addition, this pattern has also been
352 observed by others with unrelated proteins: Posfai and coworkers observed upregulation of
353 HsAQP3 in a *P. berghei* dual RNAseq study (this was confirmed in our dataset, $p = 1.81\text{x}10^{-19}$)

354 and also showed that this transporter is localized to the PVM[40]. Normally HsAQP3, a membrane
355 transporter of water and glycerol, would be trafficked to the human cell plasma membrane. The
356 host autophagosome marker, LC3, as well as other autophagosome markers, P62, NDP52, and
357 NBR1 and LAMP1 also colocalize with UIS4[41-45]. The timing of relocalization is also similar,
358 occurring here as early as 12 hours post infection, as observed for LC3[43]. While each protein that
359 was examined here and by others could have a distinct role in supporting parasite development,
360 we favor a model in which newly synthesized proteins are redirected to the vacuole and away from
361 their natural home, potentially as a universal neutralization mechanism to block cell signaling and
362 apoptosis in the infected host.

363 It has been proposed that one mechanism by which the malaria parasite may accomplish
364 the host cell remodeling is through modification of the host autophagy pathways[46]. Here the host
365 cell is relatively passive, and the parasite now directs the formation of lysosomes which are used
366 to capture pieces of the host cytoplasm and redirect them toward the parasite. This has been termed
367 the *Plasmodium*-associated autophagy-related (PAAR) response[46]. Support for this model comes
368 from the demonstration that many autophagosome markers colocalize with the PVM and some are
369 also needed for parasite development[46]. However, this does not explain why a variety of
370 completely unrelated proteins, including MUC13, AQP3[40], NR4A3 or CXCL2, all show the same
371 behavior. This model, which is based on what is observed in infected erythrocytes, does not
372 necessarily take into account the massive transcriptional changes which are observed in infected
373 hepatocytes. This autophagy model also suggests that lysosome cargo that is directed to the PV
374 consists of digested proteins.

375 We propose an alternative but possibly complementary model in which newly synthesized
376 host proteins are now secreted into the PV because the host secretion apparatus has been
377 extensively modified. This model is supported by the fact that many of the antibodies we have
378 used in our study are to full length proteins and their appearance in the PVR is associated with
379 their transcriptional upregulation in the infected host cells. Our model is also based on our
380 micrographs as well as those of others[47-49] showing that the endoplasmic reticulum (ER) is also
381 relocalized to the PVR. In fact, the upregulation and association of HsGOLGA8A with the PVR
382 may be a consequence of the relocalization of the ER and Golgi apparatus around the PV and may

383 be the easiest to understand in light of recent reports showing that the Golgi and ER move from
384 around the host nucleus in uninfected cells to around the parasite[47-49].

385 Most of the proteins that we examined bear signal sequences that would direct them to the
386 ER and Golgi. On the other hand, HsNR4A3, which presumably does not bear a signal sequence,
387 would normally be translated in the cytoplasm and imported to the nucleus via the nuclear pore
388 complex (NPC) by virtue of its nuclear localization signal. In early stages of the infection,
389 HsNR4A3 is found in the nucleus and only later relocates to the PV. Do nuclear pore proteins
390 somehow relocate from the nuclear membrane to the PVM? It is possible that nuclear pore complex
391 proteins find their way to the PVM, as well. It was recently shown that infection with LS parasites
392 results in the host microtubule organizing center (MTOC) relocalizing to the PVM. The authors of
393 the paper suggested that during infection MTOCs reorganize the host microtubule network around
394 the developing LS parasites[50]. It may be that there is an active contact site between the host nucleus
395 and the PVM through the NPCs. Active contact sites between nucleus and mitochondria[51] or
396 multiple inter-organelle contact sites[52] have been shown in mammalian cells.

397 Despite questions about how it occurs, the redirection of transcription factors away from
398 the host nucleus into to the PV could provide physiological advantages to the parasite. It could
399 render the infected cell less able to transcriptionally respond to external stimuli such as signals to
400 divide, differentiate, or undergo apoptosis, all of which would likely be unfortunate events for the
401 parasite. This could be particularly important for cells that must harbor hypnozoites for many
402 years. The redirection of HsNR4A3 away from the nucleus could also have consequences for
403 immune evasion. Proliferation and IL-2 production levels of T cells cocultured with HsNR4A3
404 knocked-down DCs were significantly lower than that of T cells cocultured with control DCs[53].

405 In contrast, HsCGA, HsMUC13, and HsCXCL2 are all secreted proteins (one membrane
406 localized and two not) and would presumably be trafficked via the endoplasmic reticulum to the
407 Golgi apparatus where they would be packaged into secretory vesicles for export. Further work
408 and mutagenesis of reporters may be needed to determine whether there are specific signals that
409 result in export to the PVM or PV.

410 The redirection of secretory vesicles to the PV versus to the extracellular space or cell
411 membrane in infected cells could have strong immunological consequences. A number of human

412 cytokines and proteins from the fever-causing NLRP3 inflammasome[54] including ATM, CDCA8,
413 CXCL10, CXCL2, ESPL1, H2AFX, HMOX1, LIG1, MDM2, NFKBIE, OGG1, PRIM1, PTTG1,
414 RAD50, RAD51, RELB, TDP1, TP53, TYMS, and XRCC1 are differentially regulated in late
415 infected hepatocytes via pathway analysis ($p = 0.0093$) and the redirection of secreted proteins to
416 the PV could be a mechanism to both improve parasite nutrition and evade host immune responses.
417 The antigens that would normally be displayed on the major histocompatibility complex on the
418 infected hepatocyte cell surface and present parasite antigens to T cells are now being secreted into
419 the PV space, where they cannot be recognized by CD8+ T cells.

420 Although both infected and uninfected cells were treated identically in our expression
421 dataset, the use flow sorted hepatoma cells, could create artefactual patterns. Recently a single cell
422 RNA-seq study was published[55]. Although a comprehensive comparison of the mouse and human
423 transcriptomes is outside the scope of this study, the patterns in our cell culture dual RNAseq
424 dataset are supported by single RNA-seq data from mouse liver infected with *P. berghei*. In
425 general, both datasets showed upregulation of genes involved in immune modulation and
426 decreased expression of metabolism associated genes. The single cell mouse study shows that
427 MmNR4A3 is clearly upregulated in infected mouse hepatocytes ($q = 9.18928E-06$) as is
428 MmCXCL2 ($q = 0$).

429 The reason for clinical silence of the malaria parasite infected liver cells has long been a
430 source of discussion. Bertolino and Bowen speculated that one reason CD8+ T cells poorly
431 recognize infected hepatocytes in a natural infection is because of either the low numbers of
432 infected hepatocytes, or because of natural tolerance[56]. An alternative explanation is that secretion
433 is modified in infected cells to direct products to the PV, as supported by our data. Our data may
434 also explain why irradiated sporozoites, which can complete the early stages of invasion but do
435 not progress to liver schizonts could create a better immune response. It would be interesting to
436 evaluate the distribution of organellar markers such as HsBiP, and HsGOLGA8A with irradiated
437 sporozoites.

438 How the parasite accomplishes host cell remodeling is unknown. Our data support the
439 Golgi as key to host cell remodeling. Much of the Golgi structure and function is controlled by
440 small Rab GTPases, which are key regulators of intracellular transport and membrane trafficking

441 in eukaryotic cells GTPases[57]; De Niz et al. demonstrated the functional importance of the
442 GTPases ARF1 and RAB1A, in *P. berghei* exoerythrocytic stage development, when they
443 expressed dominant negatives (with gain-of-function mutations in the nucleotide binding sites)
444 and showed that these mutants proteins caused an arrest and lower survival of the parasite in HeLa
445 cells[48]. In the related apicomplexan parasite, *T. gondii*, genetic screens have shown that the parasite
446 releases effector molecules into the host cell cytoplasm when it invades[58]. Although parasite
447 proteins that are needed for exoerythrocytic stages to develop have been identified in genome wide
448 genetic screens[59], it is not clear which of these are released into the host cell cytoplasm and which
449 are retained within the parasite. Screens of these mutants using host markers will likely be needed
450 to identify these factors.

451 One of the most interesting discoveries is that host cell remodeling is also observed in *P.*
452 *vivax* hypnozoites, as this now presents a way to disturb the PV and potentially provide a radical
453 cure. *P. vivax* hypnozoites, which presumably are not replicating their DNA and are not growing,
454 have traditionally been challenging to eliminate. The 8-aminoquinoline family of compounds that
455 can eliminate hypnozoites were discovered by injecting hundreds of macaques with random
456 compounds and testing to see which were permanently cured of malaria[60,61]. Recently, phenotypic
457 screening systems have begun to identify other types of compounds that are critical to hypnozoite
458 survival[62]. Our work shows that early-stage *P. berghei*, and *P. vivax* EEFs both redirect
459 upregulated proteins to the PVR, and this presents a way to study the process. This could
460 potentially lead to the identification of drug targets for the elusive hypnozoite.

461

462

463

464

465

466

467

468 **MATERIALS AND METHODS**

469 Note: Requests for materials should be addressed to Elizabeth A. Winzeler:
470 ewinzeler@health.ucsd.edu

471 *Parasites*

472 *P. berghei*-ANKA-GFP-Luc-SMCON (*Pb*-Luc)[63] and *P. berghei*-GFP (*Pb*-GFP)[63]
473 sporozoites were obtained by dissection of infected *Anopheles stephensi*[64,65] mosquito salivary
474 glands. Dissected salivary glands were homogenized in a glass tissue grinder and filtered twice
475 through nylon cell strainers (20µm pore size, Millipore SCNY00020) and counted using a
476 Neubauer hemocytometer. The sporozoites were kept on ice until needed. *Pb*-Luc and *Pb*-GFP-
477 infected *An. stephensi* mosquitoes were also obtained from the Insectary Core Facility at New
478 York University or from the Sporocore at the University of Georgia, Athens (Grant number R01
479 AI090141-08).

480 For *Pb*-Luc sporozoite production, female 6–8-week-old *Swiss webster* mice (UCSD
481 Vivarium) were injected with blood stage *Pb*-Luc parasites to begin the growth cycle. Animal
482 handling was conducted according to the UCSD Institutional Animal Care and Use Committee-
483 approved protocols. *An. stephensi* mosquitoes raised at UCSD insectary were allowed to feed on
484 infected mice with gametocytemia of ~10%. Dissected thorax sporozoites were isolated using a
485 standard protocol at day 14 or 15 post-blood meal. The sporozoites were washed with DMEM
486 incomplete media to remove debris from the thorax. The sporozoites were centrifuged 15,000 × g
487 for 5 min at 4°C to pellet and resuspended in the desired volume of complete medium.

488 *P. falciparum* sporozoites strain NF54 were isolated from infected *An. stephensi* mosquito
489 salivary glands. The sporozoites were isolated at TropIQ Health Sciences. Transistorweg 5, The
490 Netheherlands.

491 *Cell culture*

492 HC-04[66], Huh7.5.1[67] and HepG2-A16-CD81^{EGFP} [68,69] cells were cultured at 37°C with 5%
493 CO_2 in complete media (DMEM (Invitrogen, Carlsbad, USA) supplemented with 10% FBS,
494 0.29mg/mL glutamine, 100 units of penicillin, and 100µg/mL streptomycin). During and after the
495 infection with *Pb*-Luc, or *Pb*-GFP, or *P. vivax* sporozoites, complete DMEM media was

496 supplemented with antibiotics 50µg/mL gentamycin, 50µg/mL neomycin, 100 units of penicillin,
497 and 100µg/mL streptomycin, also antimycotics 50µg/mL 5-fluorocytosine, 100µg/mL
498 posaconazole and 100µg/mL neomyxin. All cell lines and source are described in Table S1.

499 *Infection of hepatocytes for qRT-PCR*

500 Hepatocytes were seeded into 24-well plates (120,000 cells per well) 24h before infection,
501 and infected with *Pb*-GFP sporozoites obtained from freshly dissected and infected *An. stephensi*
502 mosquitoes at a ratio of 0.3 sporozoites per seeded cell. Plates were centrifuged at 330 × g for 3
503 min to bring sporozoites closer to cells, and plates were then incubated at 37°C in 5% CO_2 for 2h
504 to promote sporozoite invasion[70]. After 2h, the cells were washed, fresh complete DMEM media
505 were supplemented with 12µM 5-fluorocytosine (Cayman, #11635), 50µg/mL gentamicin sulfate
506 (Gibco, #15710072), and 100µg/mL neomycin trisulfate salt hydrate (Sigma-Aldrich, #72133),
507 and the cells were returned to the incubator.

508 *Separation of infected and uninfected hepatocytes, RNA isolation and gene expression*
509 *quantification by qRT-PCR*

510 HepG2, Huh7.5.1 and HC-04 cells, in addition to primary human hepatocytes, were
511 dissociated from plates at time zero (uninfected hepatocytes and sporozoites before infection), 24
512 and 48hpi by the addition of 500µL TrypLE Express (1×, ThermoFisher, #12605010), washed
513 once using 1× PBS (Gibco, #14190144) and resuspended in FACS buffer (1× PBS supplemented
514 with 1mM EDTA, 25mM HEPES and 0.5%FBS), then passed through a 40µm cell strainer prior
515 to sorting (BD Falcon). Uninfected and infected cells were isolated by FACS using a BD Influx
516 cell sorter with GFP mean fluorescence intensity (MFI) used to determine infection status. Overall
517 gating strategy is as previously reported[17], and shown in Fig. S11 with total cells identified via
518 Forward Scatter (FSC) vs Side Scatter (SSC) (P1 gate), individual cells identified via tandem
519 gating of FSC-Height vs FSC-width and SSC-Height vs SSC-Width (gates P2 and P3), then GFP
520 positive and negative cells were collected as indicated (gates P4, and P5 respectively). For RNA
521 extraction, cells were directly sorted into Eppendorf tubes containing 600µL Qiazol reagent
522 (Qiagen) and total RNA was extracted using the Qiagen miRNEasy Mini kit (Qiagen, #217004)
523 according to manufacturer's instructions. Gene expression differences were measured using SYBR
524 green qRT-PCR with PerfeCTa SYBR® Green FastMix (Quanta Bio, #95054), using the primers

525 indicated in Table S2, and a Bio-Rad CFX96 qRT-PCR system (Bio-Rad). Changes were
526 quantitated according to the ΔΔCT method and normalized using Human Beta-2-Microglobulin
527 (*B2M*) gene.

528 *Dual RNA-sequencing analysis and code availability*

529 We analyzed the gene differential expression using data previously generated and obtained
530 in our group[17]. Reads can be found in the short read archive (http://www.ncbi.nlm.nih.gov/sra),
531 under accession number PRJNA390648. We took the dual RNA-seq read count tables from the
532 same study, and used DESeq2[71] with a multifactorial design, to calculate gene differential
533 expression at both 24 and 48h for infected versus uninfected cells, in HepG2s, Huh7.5.1s and HC-
534 04s cell lines as well as using HC-04 cells alone.

535 *Determination of infection in hepatocytes through RNA quantification by qRT-PCR*

536 Quantification of *Pb*-Luc infection was as previously described[72]. Briefly, 90,000 HC-04
537 HsNR4A3 WT and CRISPR/*Cas*9 edited cells were plated 24h before infection in 24-well plates.
538 *Pb*-Luc parasites were added at a 1:2 ratio and complete DMEM media was changed 2h later.
539 After 48h, infected cells were harvested and washed gently with PBS. RNA was isolated using
540 Qiagen miRNEasy Mini Kit (Qiagen, #217004) according to manufacture instructions. RNA was
541 quantified using a Nanodrop (Thermo Scientific) and cDNAs were synthetized using
542 SuperScript™ II Reverse Transcriptase kit (Invitrogen, #18064022). Gene expression levels for
543 parasite 18S RNA were then assessed by SYBR green qRT-PCR using perfecta SYBR Green
544 FastMix (Applied Biosystems, #4367659), the set of primers described in Table S2, a Bio-Rad
545 CFX Real-Time PCR system and quantitated using the ΔΔCT method and normalized against
546 Human Hypoxanthine phosphoribosyltransferase 1 (*HPRT1*) gene.

547 *Western blot of CRISPR/Cas9 edited cell lines*

548 Cells were first plated, infected, and sorted for GFP as described above. After sorting,
549 1,000 infected or 150,000 uninfected cells were washed twice with cold 1× PBS. Cells were lysed
550 via the addition of 200µL RIPA buffer (Teknova, #R3792) plus 1:100 protease inhibitor (Halt –
551 Thermo Fisher Scientific, #78429). Equal numbers of cells were loaded onto the gel in 2× Laemmli
552 Buffer (BioRad, #1610737), and proteins were loaded onto 18-well BioRad anyKD Criterion TGX
553 gels (Bio-Rad, #5671124). For validation of HsNR4A3 protein knockout, 10µg of protein from

554 uninfected HC-04 WT and CRISPR/*Cas*9 edited cell lines were lysed in RIPA buffer as above and
555 loaded into identical gels.

556 Approach 1: Proteins were transferred to membranes and were probed with α-HsNR4A3
557 (dilution 1:100; HsNR4A3-Ab1), and α-HsVinculin (dilution 1:100; #ab129002) antibodies
558 overnight at 4°C, probed with goat α-mouse HRP (dilution 1:5,000; #7076P2) and goat α-rabbit
559 HRP secondary (dilution 1:5,000; #G-21234) respectively, and detected using Super Signal West
560 Pico, and Femto Chemiluminescent Substrate (Thermo Fisher, #34577 and #34090). Densitometry
561 was calculated using ImageJ (http://rsbweb.nih.gov/ij/) after image inversion and is shown relative
562 to loading control.

563 Approach 2: Proteins were transferred to membranes and were probed with α-HsNR4A3
564 (dilution 1:100; HsNR4A3-Ab1), and α-HsVinculin (dilution 1:100; #4650S) antibodies overnight
565 at 4°C, probed with goat α-mouse HRP secondary (dilution 1:5,000; #7076P2) or goat α-rabbit
566 HRP secondary (dilution 1:5,000; #7074S), and detected using SuperSignal West Pico and Femto
567 Chemiluminescent Substrate (Thermo Fisher, #34577 and #34095), images were acquired using a
568 gel documentation and analysis system (Syngene, G:Box) and the software Gen Sys V.1.4.3.0.
569 Densitometry was calculated using ImageJ (http://rsbweb.nih.gov/ij/) after image inversion and is
570 shown relative to loading control.

571 *Plasmodium exoerythrocytic form (EEF) culture for cellular localization*

572 For *Pb*-Luc imaging, 96-well glass bottom plates (MatTek Corporation) or 8-well Nunc
573 Lab-Tek slides (Thermo Scientific, #125658) were coated with Poly-L-Lysine 0.01% (v/v)
574 (Sigma, #P4707) and subsequently seeded with HC-04 cells (2,500 or 25,000 cells per well,
575 respectively) 24h before infection. *Pb*-Luc sporozoites were freshly isolated from infected *An.*
576 *stephensi* mosquitoes as above and resuspended in screening DMEM media (DMEM media
577 supplemented with 5% FBS, 1.46mg/mL glutamine, 500 units of penicillin, and 500µg/mL
578 streptomycin), and additionally we added 0.5µM posaconazole (Cayman), 12µM 5-fluorocytosine
579 (Cayman), 50µg/mL gentamicin sulfate (Gemini Bio-Products), and 100µg/mL neomycin
580 trisulfate salt hydrate (Sigma-Aldrich). Pre-seeded well plates were infected with *Pb*-Luc
581 sporozoites using a 1:2 infection ratio (sporozoite to cell) and incubated for 2h at 37°C in 5% CO_2.
582 After 2h infection, medium was replaced, and plates were incubated for 48h.

583 *P. falciparum experiments*

584 Sixty thousand human primary hepatocytes were seeded in 60 wells of a collagen-coated
585 96-well microtiter plate. Two days after seeding, cells were infected with fifty thousand
586 sporozoites of *Plasmodium falciparum* strain NF54 (isolated from infected *An. Stephensi*
587 mosquitos). Five days post-infection, cells were fixed with methanol, permeabilized, blocked,
588 incubated with different primary antibodies, and evaluated by immunofluorescence and confocal
589 microscopy.

590 *P. vivax experiments*

591 *P. vivax* sporozoites were isolated from infected *An. darlingi* mosquitoes from a laboratory-
592 established colony in the Peruvian Amazon region[73,74]. Briefly, 30 patients (18 years and older)
593 from the Iquitos region, who were diagnosed with *P. vivax* malaria by blood smear and who had
594 not received treatment yet were enrolled. Approximately 20mL of whole blood was collected.
595 After centrifugation at 500 × *g* for 5 min at 37°C, plasma was removed from the *P. vivax*-infected
596 packed red cells and replaced with an equal volume of heat inactivated O^+ plasma. Then the red
597 cells were used to feed fasted female *An. darlingi* mosquitoes using a standard membrane feeding
598 assay as previously described[73,74]. After seven days, a group of ten mosquitos were midgut
599 dissected and stained by mercurochrome to evaluate oocyst development, and 14 days after the
600 first infection mosquitoes were dissected to obtain sporozoites. Dissected salivary glands were
601 homogenized in a 1.5mL tube, crushed with a homogenizer, filtered twice using nylon cell strainers
602 (20µm pore size, Millipore SCNY00020), centrifuged, and resuspended in a 500µL final volume.
603 The number of sporozoites were counted using Neubauer hematocytometer. The sporozoites were
604 kept on ice until needed.

605 For Western blot assays, 6-well glass bottom plates (Thermo Scientific, #NUNC-140675)
606 were coated with Poly-L-Lysine 0.01% (v/v) (Sigma, #P4707) and seeded with HC-04 WT cells
607 (800,000 cells per well) 24h before *P. berghei* or *P. falciparum* NF54 sporozoites infection
608 (400,000 sporozoites per well). *P. berghei* or *P. falciparum* NF54 were diluted in DMEM media
609 using 1:2 infection ratio (sporozoites to HC-04 cells) and incubated 4h at 37°C under 5% CO_2
610 atmosphere. After this initial incubation period, infection media was replaced with fresh screening
611 DMEM media, plates with HC-04 cells infected with *P. berghei* were incubated for two days, and

612 the plates with HC-04 cells infected with *P. falciparum* were incubated for five days, the screening
613 DMEM media was replaced every 24h.

614 Uninfected and infected cells were lysed via the addition of 200µL RIPA buffer (Fisher
615 Scientific, #P189900) plus protease inhibitor cocktail (cOmplete Mini, EDTA-free – Roche,
616 #11836170001). Proteins (50µg) were mixed with 4× Laemmli Buffer (BioRad, #1610737), and
617 loaded onto 12-well BioRad Criterion TGX gels (Bio-Rad, #5671083). Proteins were transferred
618 to nitrocellulose membranes and were different primary antibodies overnight at 4°C (Table S2),
619 probed with goat α-mouse HRP secondary antibody (dilution 1:2,000; #7076P2), goat α-rabbit
620 HRP secondary antibody (dilution 1:2,000; #7074S) or rabbit α-goat HRP secondary antibody
621 (dilution 1:2,000; #A27014), and detected using SuperSignal West Pico or Femto
622 Chemiluminescent Substrate (Thermo Fisher, #34577 and #34095), images were acquired using a
623 gel documentation and analysis system (Syngene, G:Box) and the software Gen Sys V.1.4.3.0.

624 For IFA analysis 96-well glass bottom plates (MatTek Corporation) or 8-well Nunc Lab-
625 Tek chamber slides (Thermo Scientific, #125658) were coated with Poly-L-Lysine 0.01% (v/v)
626 (Sigma, #P4707) and seeded with HC-04 WT or CRISPR/*Cas*9 edited cells (2,500 or 25,000 cells
627 per well) 24h prior to mosquito dissection and infection. *P. vivax* sporozoites were diluted in
628 screening DMEM media (supplemented as above). Slides were infected using a 1:2 infection ratio
629 (sporozoites to HC-04 cells) and incubated for 4h at 37°C under 5% CO_2 atmosphere. After this
630 initial incubation period, infection media was replaced with fresh screening DMEM media, and
631 plates or slides were incubated for five days, the screening DMEM media was replaced every 24h.

632 *Plasmodium EEF and HsNR4A3 immunofluorescence microscopy and high content imaging*

633 All primary and secondary antibodies used in this study are given in Table S3-S5. We used
634 HC-04 HsNR4A3 wild type cells (HC-04 wild type), CRISPR/*Cas*9 edited cells lines (NM1, NM2
635 and NM3 or GL1, and GL3) and the *Pb*-Luc parasites[75]. The different cells lines were seeded in
636 8-well chamber slides and infected them with a 1:2 infection ratio (sporozoite to HC-04 cell). After
637 48h of infection, cells were fixed with 4% paraformaldehyde-PBS (Affymetrix, #19943) for 20
638 min at RT, permeabilized with 0.1% TritonX-100 (Fisher, #BP151500) for 10 min at RT, blocked
639 with 1% BSA for 1h and incubated with two antibodies overnight at 4°C. The first antibody was a
640 α-PvUIS4 or α-PbUIS4 (mouse monoclonal antibody for *P. vivax* UIS4 or goat polyclonal

641 antibody for *P. berghei* UIS4; dilution 1:500; α-PvUIS4 antibody donated by Kappe's Lab or α-
642 PbUIS4 antibody, #LS-C204260), and for human host proteins the following set of antibodies were
643 used: α-HsNR4A3 (dilution 1:100; HsNR4A3-Ab1), α-HsCGA (dilution 1:50; HsCGA-Ab1), α-
644 HsGOLGA8A (dilution 1:50; HsGOLGA8A-Ab1), or α-HsMUC13 (dilution 1:50, HsMUC13-
645 Ab1). Then, the following secondary antibodies were used for plasmodium parasites (PvUIS4 or
646 PbUIS4) 1) Donkey α-mouse (dilution 1:1,000; #715297003) or bovine α-goat (dilution 1:1,000;
647 #805297008), Rhodamine Red™-X - Red, and for the human host proteins: 2) Donkey α-mouse
648 or goat α-rabbit (dilution 1:1,000; #A32766, or #111545046, Alexa Fluor 488 - Green) and
649 incubated for 2h at RT. Hepatocyte plasma membrane was detected using CellMask deep red
650 (Thermo Fisher Scientific, #C10046) at 1×. After IFA, chambers were removed from *Pb*-Luc-
651 infected Lab-Tek systems, slides were mounted with Vectashield with DAPI (Vector Labs, #H-
652 1500) and #1.5 glass coverslips were affixed using nail polish. Images were acquired using a Zeiss
653 LSM880 with Airyscan Confocal Microscope (63× Plan-Apochromat /1.4 NA DIC oil immersion
654 objective); laser power was set to 3% for 405, 488, 561, and 640nm. The images were processed
655 using the confocal ZEN software (Black edition, Zeiss). The level of colocalization between the
656 two fluorescent proteins (α-PbUIS4/α-HsNR4A3, α-PvUIS4/α-HsCGA, α-PvUIS4/α-
657 HsGOLGA8A, α-PvUIS4/α-HsMUC13, or α-PbUIS4/α-HsCXCL2 were determined by
658 calculating the product of the difference from the mean (PDM) indicated a mean Pearson
659 coefficient r (Pearson correlation coefficient - PCC) in PV, α-PbUIS4 or α-PvUIS4 was on channel
660 A vs human host protein on channel B. The PCC were analyzed using Volocity 3D/4D rendering
661 software for three identified objects from each of three biological replicates.

662 *Ultrastructure Expansion Microscopy (U-ExM)*

663 Clean coverslips (Fisher Scientific, #NC1129240) pretreated with poly-l-lysine for 1h at
664 37°C, washed with MilliQ water, dried, and placed in the wells of a 12-well plate, were used to
665 seed human liver cells (HC-04 or Huh7.5.1 cells, 200,000) resuspended in 1ml of DMEM complete
666 media and incubated at 37°C, 5% CO_2, for 24h. The infection was performed with *P. berghei*
667 sporozoites (100,000) at ratio 2:1 (two cells to one parasite), incubated during 48h, 37°C, 5% CO_2.
668 Supernatants were removed, and the cells were fixed with 1 mL of 4% PFA (EMS #15710)/PBS
669 for 20 min at 37°C. then stored and shipped overnight to the Absalon laboratory at Indiana

670 University School of Medicine. At reception, coverslips were proceeded for expansion microscopy
671 as described in Liffner and Absalon 2021[38]. Gels were incubated overnight with primary antibodies
672 with the following dilution 1:250 for α-PbUIS4 (#LS-C204260), and 1:100 for α-HsNR4A3
673 (HsNR4A3-Ab1) at room temperature on a shaker. All secondary antibodies were diluted 1:500 in
674 PBS (donkey anti-goat-Alexa 488, ThermoFisher Scientific #A-11055 and donkey anti-mouse-
675 Alexa 555, ThermoFisher Scientific #A-31570), 1:250 for NHS ester-Alexa 405 (ThermoFisher
676 Scientific #A7573) and 1:1000 for Sytox™ Deep red (ThermoFisher Scientific #S11380) and
677 incubated room temperature on a shaker for 2h and 30 min. Staining with 1:1000 Bodipy-TR-
678 Ceramide (ThermoFisher Scientific #D7540) required an additional overnight room temperature
679 on a shaker.

680 For imaging, small sections of the larger gel were cut and gently dried before being placed
681 into 35 mm #1.5 coverslips bottomed imaging dishes (Cellvis; Fisher Scientific #NC0409658)
682 precoated with poly-D-lysine. The images were acquired using a Zeiss LSM900 AxioObserver
683 microscope with Airyscan 2 detector, with 63x Plan-Apochromat (NA 1.4) objective lens. All
684 images were acquired in multiplex mode 2 as Z-stacks with and XY pixel size 0.035 µm and a Z-
685 step size of 0.13 µm, and processed using Zen Blue software (Version 3.5, Zeiss, Oberkochen,
686 Germany).

687 *High content imaging (HCI) of edited lines*

688 HC-04[66] CRISPR/*Cas*9 edited cell lines were seeded in 384-well plates or 8-well Lab-Tek
689 slides and infected with *Pb*-Luc parasites[63] at a ratio 2:1 (cells/sporozoites). After 48h cells were
690 fixed, permeabilized, blocked and incubated with α-PbUIS4 (dilution 1:500; #LS-C204260) and
691 α-HsNR4A3 (dilution 1:100; HsNR4A3-Ab1), and visualized using bovine α-goat
692 (#805297008, Rhodamine Red) and donkey α-mouse (#A32766, Alexa Fluor 488 - Green)
693 secondary antibodies. The data were acquired (image analysis) using a High Content Imaging
694 System (Operetta®, PerkingElmer). PbUIS4 protein was detected using the 568 channel (excitation
695 560-580nm, emission 590-640nm), exposure time of 200ms, and height of 82µm. HsNR4A3
696 protein was detected using the 488 channel (excitation 460-490nm, emission 500-550nm) with
697 exposure time 200ms and height 82µm. Plasma membranes were detected using the DRAQ5
698 channel (excitation 620-640nm, emission 650-760nm) with exposure time of 200ms and a height

699 80µm. Nuclei (DAPI) were detected using an excitation wavelength of 360-400nm, emission 410-
700 480nm, with exposure time at 200 milliseconds (ms), and a height 40µm.

701 To evaluate and determined the size of *P. berghei* schizonts forms we use a splitting
702 coefficient of 0.40; common threshold, 0.40, split factor 72.0; individual threshold, 0.50; contrast,
703 0.50. Schizonts were also evaluated using different sets for diameter: 5, 20, 30 and 40µm^2. The
704 images were captured using a 10× long WD/0.3 NA objective, 10× magnification, 10 fields, 1
705 plane and 1 time point.

706 *Cytokine HsCXCL2 stimulation with lipopolysaccharide (LPS)*

707 To evaluate the expression of human chemokine HsCXCL2 (GROß), *in vitro* infections
708 were performed using the human liver line HC-04 with *P. berghei* sporozoites in 8-well Lab-Tek
709 slides. Cells were stimulated by treatment with 1µg/mL lipopolysaccharide (LPS), from *E. coli*
710 O55: B5 (Sigma Aldrich, # L6529). Cells were treated with different periods of exposition to LPS
711 (2, 24 and 48hpi), fixed and collected for confocal microscopy. The expression and localization
712 of HsCXCL2 protein in HC-04 cells were visualized through the use of the α-HsCXCL2 primary
713 antibody (dilution 1:100; HsCXCL2-Ab1). *P. berghei* parasites were visualized α-PbUIS4
714 polyclonal antibody (dilution 1:500; #LS-C204260), and their respective secondary antibodies
715 (dilution 1:1,000; #711296152 and #705546147). Plasma membranes were detected using
716 CellMask deep red, and nucleus were stained with DAPI.

717 *HsNR4A3 CRISPR/Cas9 (Approach 1)*

718 HsNR4A3 was edited using a sequential two plasmid CRISPR/*Cas9* approach. First, HC-
719 04 cells expressing CAS9 were generated using lentivirus containing the EF1a-*Cas9*-2A-
720 Blasticidin Lenti plasmid (Sigma Aldrich, #LVCAS9BST-1EA). HC-04 cells were plated at a
721 density of 120,000 cells per well in three independent wells of a 24 well plate. Twenty-four hours
722 after plating, media was replaced with complete media (as above) plus 5µg/mL polybrene and viral
723 particles. Cas9 lentiviral particles were added at a multiplicity of infection (MOI) of 0.5, after
724 which cells were spun at 800 × g for 30 min, then incubated overnight at 37°C. The following day
725 media, was changed to complete media and cells were again incubated overnight at 37°C. The
726 next day, cells were selected for presence of the CAS9 plasmid using complete media plus
727 2.5µg/mL blasticidin (Thermo Fisher, #A1113903). After 14 days of selection, splitting as

728 required, cells were trypsinized and plated at an average density of one cell per well in a 96 well
729 plate in complete media plus blasticidin as above. Once cells had regrown, wells were observed
730 via microscopy to identify those wells which appeared to contain single colonies. CAS9
731 expression within clones was then confirmed via PCR.

732 Once CAS9 expressing HC-04 cells were established, gRNA targeting *HsNR4A3* was
733 introduced via Lentivirus containing the LV04 U6-gRNA:hPGK-Puro-2A-BFP plasmid and a
734 gRNA sequence specific for Human *HsNR4A3*. The DNA sequence targeted by the gRNA for
735 *HsNR4A3* was CTGCAGCAGCCTGGTCAGTGGG (Sigma-Aldrich Sanger Clone ID
736 HS5000010424). Cells were infected with virus and cultured overnight as above. The following
737 day, cells were selected for presence of the gRNA plasmid using complete media plus 2.5µg/mL
738 puromycin (Gibco, #A1113803) and 2.5µg/mL blasticidin. Clonal cell lines expressing the gRNA
739 and CAS9 were generated as previously stated. The presence of *HsNR4A3* knockout within these
740 apparent monoclonal HC-04 cell lines was examined at the protein level, after being expanded into
741 25cm^2 vented tissue culture flasks, via western blot using the HsNR4A3 rabbit polyclonal antibody
742 (dilution 1:100; HsNR4A3-Ab1). Three edited clones (clones GL1, GL2, and GL3) were then
743 examined using confocal microscopy, all exhibited low or no host cell HsNR4A3 protein
744 expression.

745 *HsNR4A3 CRISPR/Cas9 (Approach 2)*

746 A second round of editing for *HsNR4A3* was performed using a single plasmid
747 CRISPR/*Cas9* system with the Edit-R All-in-one Lentiviral an sgRNA, targeting *HsNR4A3*,
748 packaged in a lentiviral vector (Horizon, Perkin Elmer). The gRNA sequence used was
749 TTCGACGTCTCTTGTCTACT, targeting exon 5 of *HsNR4A3* coding sequence. Briefly, HC-04
750 cells were plated at a density of 150,000 cells per well in a 6 well plate, then 24h later media was
751 replaced with complete media supplemented with 10µg/mL polybrene. Virus was added at a
752 multiplicity of infection of one and then incubated overnight at 37°C. After 48h, the cells were
753 selected for presence of the CAS9 plasmid using complete media plus 2.5µg/mL puromycin. After
754 seven days of selection, cells were trypsinized and plated at an average density of 0.5 cell per well
755 in a 96-well plate in the presence of 2.5µg/mL puromycin for clonal selection. After ~15-20 days,
756 wells were observed via microscopy to identify those wells which contained single colonies. These

757 cells were then transferred to 6-well plates and the knockout of HsNR4A3 was confirmed in these
758 apparent monoclonal HC-04 cell lines with immunoblotting.

759 Since, in the above obtained clones, there was only partial knockout of HsNR4A3, another
760 round of transductions was performed using guide RNA GCTCGAGTAGCCCTCCACGA
761 targeting at exon 4. Lenti-V2-Blast (lentiCRISPR v2-Blast plasmid, Addgene) plasmid was used
762 here. Transductions were performed, as mentioned above, and the transformed cells were selected
763 using 1µg/mL blasticidin and 2.5µg/mL puromycin. The clones obtained after clonal selection
764 were evaluated for HsNR4A3 expression by immunoblotting using the HsNR4A3 mouse
765 monoclonal antibody (dilution 1:100; HsNR4A3-Ab1). Three knockdown clones (clones NM1,
766 NM2, and NM3) were selected to have low HsNR4A3 expression. These clones were then used
767 for further studies.

768 ETHICS STATEMENT

769 Human subject protocols were approved by the Human Research Protection Program of
770 the University of California, San Diego (approval number 120652) and Universidad Peruana
771 Cayetano Heredia (approval number 102357). Written informed consent was obtained from all
772 study participants.

773 ACKNOWLEDGMENTS

774 We thank the members of the Winzeler laboratory for advice and critical reading of the
775 manuscript. In addition, we thank Medicines for Malaria Venture and Fogarty International Center
776 of the National Institutes of Health (NIH) under Award Number D43TW009343 and the University
777 of California Global Health Institute (UCGHI) for all their support of the insectary in Peru. We
778 would also like to thank the UCSD Human Embryonic Stem Cell Flow Cytometry Core Facility,
779 and UCSD Microscopy Core – NINDS NS047101 for their technical support. JC was supported
780 by the Fogarty International Center of the National Institutes of Health (NIH) under Award
781 Number D43TW009343 and the University of California Global Health Institute (UCGHI). GL
782 was supported by an A.P. Giannini Post-Doctoral Fellowship. EAW is supported by grants from
783 the NIH (1R01AI152533 and R01AI103058), and MMV. The *P. vivax* work was supported by

grants to JMV from the NIH (D43TW007120 and U19AI089681) and MMV. GTW was supported by NIH training grant T32AI007036. M.R. lab funded by the NIH grants AI126277, AI145325, AI154644, AI114625, by the Chiba University-University of California-San Diego (UCSD) Center for Mucosal Immunology, Allergy, and Vaccines, and by the UCSD Department of Pediatrics. M.R. also holds an Investigator in the Pathogenesis of Infectious Disease Award from the Burroughs Wellcome Fund.

AUTHOR CONTRIBUTIONS

JC performed Immunofluorescence, HCI, qRT-PCR, Western blot assays and data analysis. GL infected and sorted liver cells, isolated RNA for both infected and uninfected populations and measured gene expression levels via qRT-PCR and Western blot. JC and LG performed *P. vivax* liver stage assays. GL, BYZ, EP and NM generated *HsNR4A3* edited cell lines. JC, GL, and EW wrote the manuscript. KPGM analyzed data and created figures. BC contributed concepts and helped fund the study. CTR, DG and JV developed methods and infrastructure for *P. vivax* infections. GTW performed ELISA assays for HsCXCL2 protein. SA and BL performed U-ExM and imaging. All authors assisted with editing of the manuscript. The authors declare no conflicts of interest or competing financial interests.

REFERENCES

1 Fodor, S. P. *et al.* Multiplexed biochemical assays with biological chips. *Nature* **364**, 555-556 (1993).

2 Pradel, G. & Frevert, U. Malaria sporozoites actively enter and pass through rat Kupffer cells prior to hepatocyte invasion. *Hepatology* **33**, 1154-1165 (2001). https://doi.org:10.1053/jhep.2001.24237

3 Barnwell, J. W. Hepatic Kupffer cells: the portal that permits infection of hepatocytes by malarial sporozoites? *Hepatology* **33**, 1331-1333 (2001). https://doi.org:10.1053/jhep.2001.24740

4 Frischknecht, F. & Matuschewski, K. Plasmodium Sporozoite Biology. *Cold Spring Harb Perspect Med* **7** (2017). https://doi.org:10.1101/cshperspect.a025478

5 Mota, M. M., Hafalla, J. C. & Rodriguez, A. Migration through host cells activates Plasmodium sporozoites for infection. *Nat Med* **8**, 1318-1322 (2002). https://doi.org:10.1038/nm785

6 Sinai, A. *The Toxoplasma gondii Parasitophorous Vacuole Membrane: A multifunctional Organelle in the Infected Cell*. (2014).

7 Markus, M. B. Malaria: origin of the term "hypnozoite". *J Hist Biol* **44**, 781-786 (2011). https://doi.org:10.1007/s10739-010-9239-3

8 Vaughan, A. M. & Kappe, S. H. I. Malaria Parasite Liver Infection and Exoerythrocytic Biology. *Cold Spring Harb Perspect Med* **7** (2017). https://doi.org:10.1101/cshperspect.a025486

9 Wilby, K. J., Lau, T. T., Gilchrist, S. E. & Ensom, M. H. Mosquirix (RTS,S): a novel vaccine for the prevention of Plasmodium falciparum malaria. *Ann Pharmacother* **46**, 384-393 (2012). https://doi.org:10.1345/aph.1AQ634

10 Casares, S., Brumeanu, T. D. & Richie, T. L. The RTS,S malaria vaccine. *Vaccine* **28**, 4880-4894 (2010). https://doi.org:10.1016/j.vaccine.2010.05.033

11 Laurens, M. B. RTS,S/AS01 vaccine (Mosquirix?): an overview. *Human Vaccines & Immunotherapeutics* **16**, 480-489 (2020). https://doi.org:10.1080/21645515.2019.1669415

12 Nussenzweig, R., Vanderberg, J. & Most, H. Protective immunity produced by the injection of x-irradiated sporozoites of Plasmodium berghei. IV. Dose response, specificity and humoral immunity. *Mil Med* **134**, 1176-1182 (1969).

13 Sharma, S. & Pathak, S. Malaria vaccine: a current perspective. *J Vector Borne Dis* **45**, 1-20 (2008).

843 14 Goh, Y. S., McGuire, D. & Renia, L. Vaccination With Sporozoites: Models and Correlates
844 of Protection. *Front Immunol* **10**, 1227 (2019). https://doi.org:10.3389/fimmu.2019.01227

845 15 Leiriao, P., Mota, M. M. & Rodriguez, A. Apoptotic Plasmodium-infected hepatocytes
846 provide antigens to liver dendritic cells. *J Infect Dis* **191**, 1576-1581 (2005).
847 https://doi.org:10.1086/429635

848 16 Vaughan, A. M., Wang, R. & Kappe, S. H. Genetically engineered, attenuated whole-cell
849 vaccine approaches for malaria. *Hum Vaccin* **6**, 107-113 (2010).
850 https://doi.org:10.4161/hv.6.1.9654

851 17 LaMonte, G. M. *et al.* Dual RNA-seq identifies human mucosal immunity protein Mucin-
852 13 as a hallmark of Plasmodium exoerythrocytic infection. *Nat Commun* **10**, 488 (2019).
853 https://doi.org:10.1038/s41467-019-08349-0

854 18 Mueller, A. K. *et al.* Plasmodium liver stage developmental arrest by depletion of a protein
855 at the parasite-host interface. *Proc Natl Acad Sci U S A* **102**, 3022-3027 (2005).
856 https://doi.org:10.1073/pnas.0408442102

857 19 Bertiaux, E. *et al.* Expansion microscopy provides new insights into the cytoskeleton of
858 malaria parasites including the conservation of a conoid. *PLoS Biol* **19**, e3001020 (2021).
859 https://doi.org:10.1371/journal.pbio.3001020

860 20 McGuckin, M. A., Linden, S. K., Sutton, P. & Florin, T. H. Mucin dynamics and enteric
861 pathogens. *Nat Rev Microbiol* **9**, 265-278 (2011). https://doi.org:10.1038/nrmicro2538

862 21 Fu, Y., Luo, L., Luo, N., Zhu, X. & Garvey, W. T. NR4A orphan nuclear receptors
863 modulate insulin action and the glucose transport system: potential role in insulin
864 resistance. *J Biol Chem* **282**, 31525-31533 (2007).
865 https://doi.org:10.1074/jbc.M701132200

866 22 Reynolds, M. S. *et al.* beta-Cell deletion of Nr4a1 and Nr4a3 nuclear receptors impedes
867 mitochondrial respiration and insulin secretion. *Am J Physiol Endocrinol Metab* **311**, E186-
868 201 (2016). https://doi.org:10.1152/ajpendo.00022.2016

869 23 Close, A. F., Dadheech, N., Villela, B. S., Rouillard, C. & Buteau, J. The orphan nuclear
870 receptor Nor1/Nr4a3 is a negative regulator of beta-cell mass. *J Biol Chem* **294**, 4889-4897
871 (2019). https://doi.org:10.1074/jbc.RA118.005135

872 24 Duez, H. & Pourcet, B. Nuclear Receptors in the Control of the NLRP3 Inflammasome
873 Pathway. *Front Endocrinol (Lausanne)* **12**, 630536 (2021).
874 https://doi.org:10.3389/fendo.2021.630536

875 25 Fedorova, O. *et al.* Orphan receptor NR4A3 is a novel target of p53 that contributes to
876 apoptosis. *Oncogene* **38**, 2108-2122 (2019). https://doi.org:10.1038/s41388-018-0566-8

877 26 Casarini, L., Santi, D., Brigante, G. & Simoni, M. Two Hormones for One Receptor:
878 Evolution, Biochemistry, Actions, and Pathophysiology of LH and hCG. *Endocr Rev* **39**,
879 549-592 (2018). https://doi.org:10.1210/er.2018-00065

880 27 Bieche, I. *et al.* The CGA gene as new predictor of the response to endocrine therapy in
881 ER alpha-positive postmenopausal breast cancer patients. *Oncogene* **20**, 6955-6959 (2001).
882 https://doi.org:10.1038/sj.onc.1204739

883 28 Lu, P., Zhang, C. H., Lifshitz, L. M. & ZhuGe, R. Extraoral bitter taste receptors in health
884 and disease. *J Gen Physiol* **149**, 181-197 (2017). https://doi.org:10.1085/jgp.201611637

885 29 Zhang, P., Cao, L., Zhou, R., Yang, X. & Wu, M. The lncRNA Neat1 promotes activation
886 of inflammasomes in macrophages. *Nat Commun* **10**, 1495 (2019).
887 https://doi.org:10.1038/s41467-019-09482-6

888 30 Kim, J. *et al.* Long noncoding RNA MALAT1 suppresses breast cancer metastasis. *Nat*
889 *Genet* **50**, 1705-1715 (2018). https://doi.org:10.1038/s41588-018-0252-3

890 31 Menon, M. P. & Hua, K. F. The Long Non-coding RNAs: Paramount Regulators of the
891 NLRP3 Inflammasome. *Front Immunol* **11**, 569524 (2020).
892 https://doi.org:10.3389/fimmu.2020.569524

893 32 Liu, J. *et al.* The role of the Golgi apparatus in disease (Review). *Int J Mol Med* **47** (2021).
894 https://doi.org:10.3892/ijmm.2021.4871

895 33 Gillingham, A. K. & Munro, S. Finding the Golgi: Golgin Coiled-Coil Proteins Show the
896 Way. *Trends Cell Biol* **26**, 399-408 (2016). https://doi.org:10.1016/j.tcb.2016.02.005

897 34 Mikolajczak, S. A. *et al.* Plasmodium vivax liver stage development and hypnozoite
898 persistence in human liver-chimeric mice. *Cell Host Microbe* **17**, 526-535 (2015).
899 https://doi.org:10.1016/j.chom.2015.02.011

900 35 Nomiyama, T. *et al.* The NR4A orphan nuclear receptor NOR1 is induced by platelet-
901 derived growth factor and mediates vascular smooth muscle cell proliferation. *J Biol Chem*
902 **281**, 33467-33476 (2006). https://doi.org:10.1074/jbc.M603436200

903 36 Jakymiw, A. *et al.* Identification and characterization of a novel Golgi protein, golgin-67.
904 *J Biol Chem* **275**, 4137-4144 (2000). https://doi.org:10.1074/jbc.275.6.4137

905 37 Friesen, J. *et al.* Natural immunization against malaria: causal prophylaxis with antibiotics.
906 *Sci Transl Med* **2**, 40ra49 (2010). https://doi.org:2/40/40ra49 [pii]

907 10.1126/scitranslmed.3001058

908 38 Liffner, B. & Absalon, S. Expansion Microscopy Reveals Plasmodium falciparum Blood-
909 Stage Parasites Undergo Anaphase with A Chromatin Bridge in the Absence of Mini-

Chromosome Maintenance Complex Binding Protein. *Microorganisms* **9** (2021). https://doi.org:10.3390/microorganisms9112306

39 De Filippo, K. *et al.* Mast cell and macrophage chemokines CXCL1/CXCL2 control the early stage of neutrophil recruitment during tissue inflammation. *Blood* **121**, 4930-4937 (2013). https://doi.org:10.1182/blood-2013-02-486217

40 Posfai, D. *et al.* Plasmodium parasite exploits host aquaporin-3 during liver stage malaria infection. *PLoS Pathog* **14**, e1007057 (2018). https://doi.org:10.1371/journal.ppat.1007057

41 Agop-Nersesian, C. *et al.* Shedding of host autophagic proteins from the parasitophorous vacuolar membrane of Plasmodium berghei. *Sci Rep* **7**, 2191 (2017). https://doi.org:10.1038/s41598-017-02156-7

42 Grutzke, J. *et al.* The spatiotemporal dynamics and membranous features of the Plasmodium liver stage tubovesicular network. *Traffic* **15**, 362-382 (2014). https://doi.org:10.1111/tra.12151

43 Real, E. *et al.* Plasmodium UIS3 sequesters host LC3 to avoid elimination by autophagy in hepatocytes. *Nat Microbiol* **3**, 17-25 (2018). https://doi.org:10.1038/s41564-017-0054-x

44 Schmuckli-Maurer, J. *et al.* Inverted recruitment of autophagy proteins to the Plasmodium berghei parasitophorous vacuole membrane. *PLoS One* **12**, e0183797 (2017). https://doi.org:10.1371/journal.pone.0183797

45 Niklaus, L. *et al.* Deciphering host lysosome-mediated elimination of Plasmodium berghei liver stage parasites. *Sci Rep* **9**, 7967 (2019). https://doi.org:10.1038/s41598-019-44449-z

46 Agop-Nersesian, C., Niklaus, L., Wacker, R. & Theo Heussler, V. Host cell cytosolic immune response during Plasmodium liver stage development. *FEMS Microbiol Rev* **42**, 324-334 (2018). https://doi.org:10.1093/femsre/fuy007

47 Bano, N., Romano, J. D., Jayabalasingham, B. & Coppens, I. Cellular interactions of Plasmodium liver stage with its host mammalian cell. *Int J Parasitol* **37**, 1329-1341 (2007). https://doi.org:10.1016/j.ijpara.2007.04.005

48 De Niz, M. *et al.* Hijacking of the host cell Golgi by Plasmodium berghei liver stage parasites. *J Cell Sci* **134** (2021). https://doi.org:10.1242/jcs.252213

49 Deschermeier, C. *et al.* Mitochondrial lipoic acid scavenging is essential for Plasmodium berghei liver stage development. *Cell Microbiol* **14**, 416-430 (2012). https://doi.org:10.1111/j.1462-5822.2011.01729.x

50 Vijayan, K. *et al.* A genome-wide CRISPR-Cas9 screen identifies CENPJ as a host regulator of altered microtubule organization during Plasmodium liver infection. *Cell Chem Biol* **29**, 1419-1433 e1415 (2022). https://doi.org:10.1016/j.chembiol.2022.06.001

945 51 Eisenberg-Bord, M. *et al.* Cnm1 mediates nucleus-mitochondria contact site formation in
946 response to phospholipid levels. *J Cell Biol* **220** (2021).
947 https://doi.org:10.1083/jcb.202104100

948 52 Kakimoto, Y. *et al.* Visualizing multiple inter-organelle contact sites using the organelle-
949 targeted split-GFP system. *Sci Rep* **8**, 6175 (2018). https://doi.org:10.1038/s41598-018-
950 24466-0

951 53 Nagaoka, M. *et al.* The Orphan Nuclear Receptor NR4A3 Is Involved in the Function of
952 Dendritic Cells. *J Immunol* **199**, 2958-2967 (2017).
953 https://doi.org:10.4049/jimmunol.1601911

954 54 Swanson, K. V., Deng, M. & Ting, J. P. The NLRP3 inflammasome: molecular activation
955 and regulation to therapeutics. *Nat Rev Immunol* **19**, 477-489 (2019).
956 https://doi.org:10.1038/s41577-019-0165-0

957 55 Afriat, A. *et al.* A spatiotemporally resolved single-cell atlas of the Plasmodium liver stage.
958 *Nature* **611**, 563-569 (2022). https://doi.org:10.1038/s41586-022-05406-5

959 56 Bertolino, P. & Bowen, D. G. Corrigendum: Malaria and the liver: immunological hide-
960 and-seek or subversion of immunity from within? *Front Microbiol* **6**, 460 (2015).
961 https://doi.org:10.3389/fmicb.2015.00460

962 57 Goud, B., Liu, S. & Storrie, B. Rab proteins as major determinants of the Golgi complex
963 structure. *Small GTPases* **9**, 66-75 (2018).
964 https://doi.org:10.1080/21541248.2017.1384087

965 58 Hunter, C. A. & Sibley, L. D. Modulation of innate immunity by Toxoplasma gondii
966 virulence effectors. *Nat Rev Microbiol* **10**, 766-778 (2012).
967 https://doi.org:10.1038/nrmicro2858

968 59 Stanway, R. R. *et al.* Genome-Scale Identification of Essential Metabolic Processes for
969 Targeting the Plasmodium Liver Stage. *Cell* **179**, 1112-1128.e1126 (2019).
970 https://doi.org:10.1016/j.cell.2019.10.030

971 60 Dow, G. S. *et al.* Radical curative efficacy of tafenoquine combination regimens in
972 Plasmodium cynomolgi-infected Rhesus monkeys (Macaca mulatta). *Malar J* **10**, 212
973 (2011). https://doi.org:10.1186/1475-2875-10-212

974 61 Baird, J. K. 8-Aminoquinoline Therapy for Latent Malaria. *Clin Microbiol Rev* **32** (2019).
975 https://doi.org:10.1128/CMR.00011-19

976 62 Roth, A. *et al.* A comprehensive model for assessment of liver stage therapies targeting
977 Plasmodium vivax and Plasmodium falciparum. *Nat Commun* **9**, 1837 (2018).
978 https://doi.org:10.1038/s41467-018-04221-9

979 63 Janse, C. J. *et al.* High efficiency transfection of Plasmodium berghei facilitates novel
980 selection procedures. *Molecular and Biochemical Parasitology* **145**, 60-70 (2006).
981 https://doi.org:10.1016/j.molbiopara.2005.09.007

982 64 Rosenberg, R., Wirtz, R. A., Schneider, I. & Burge, R. An estimation of the number of
983 malaria sporozoites ejected by a feeding mosquito. *Trans R Soc Trop Med Hyg* **84**, 209-
984 212 (1990). https://doi.org:10.1016/0035-9203(90)90258-g

985 65 Medica, D. L. & Sinnis, P. Quantitative dynamics of Plasmodium yoelii sporozoite
986 transmission by infected anopheline mosquitoes. *Infect Immun* **73**, 4363-4369 (2005).
987 https://doi.org:10.1128/IAI.73.7.4363-4369.2005

988 66 Sattabongkot, J. *et al.* Establishment of a human hepatocyte line that supports in vitro
989 development of the exo-erythrocytic stages of the malaria parasites Plasmodium
990 falciparum and P. vivax. *Am J Trop Med Hyg* **74**, 708-715 (2006).

991 67 Swann, J. *et al.* High-Throughput Luciferase-Based Assay for the Discovery of
992 Therapeutics That Prevent Malaria. *ACS Infect Dis* **2**, 281-293 (2016).
993 https://doi.org:10.1021/acsinfecdis.5b00143

994 68 Yalaoui, S. *et al.* Hepatocyte permissiveness to Plasmodium infection is conveyed by a
995 short and structurally conserved region of the CD81 large extracellular domain. *PLoS*
996 *Pathog* **4**, e1000010 (2008). https://doi.org:10.1371/journal.ppat.1000010

997 69 Silvie, O. *et al.* Expression of human CD81 differently affects host cell susceptibility to
998 malaria sporozoites depending on the Plasmodium species. *Cell Microbiol* **8**, 1134-1146
999 (2006). https://doi.org:10.1111/j.1462-5822.2006.00697.x

1000 70 Prudencio, M., Rodriguez, A. & Mota, M. M. The silent path to thousands of merozoites:
1001 the Plasmodium liver stage. *Nature reviews. Microbiology* **4**, 849-856 (2006).
1002 https://doi.org:10.1038/nrmicro1529

1003 71 Love, M. I., Huber, W. & Anders, S. Moderated estimation of fold change and dispersion
1004 for RNA-seq data with DESeq2. *Genome Biol* **15**, 550 (2014).
1005 https://doi.org:10.1186/s13059-014-0550-8

1006 72 Bahamontes-Rosa, N. *et al.* New molecular settings to support in vivo anti-malarial assays.
1007 *Malar J* **15**, 147 (2016). https://doi.org:10.1186/s12936-016-1205-x

1008 73 Moreno, M. *et al.* Infection of laboratory-colonized Anopheles darlingi mosquitoes by
1009 Plasmodium vivax. *Am J Trop Med Hyg* **90**, 612-616 (2014).
1010 https://doi.org:10.4269/ajtmh.13-0708

1011 74 Moreno, M. *et al.* Continuous Supply of Plasmodium vivax Sporozoites from Colonized
1012 Anopheles darlingi in the Peruvian Amazon. *ACS Infect Dis* **4**, 541-548 (2018).
1013 https://doi.org:10.1021/acsinfecdis.7b00195

75 Franke-Fayard, B. *et al.* Simple and sensitive antimalarial drug screening in vitro and in vivo using transgenic luciferase expressing Plasmodium berghei parasites. *Int J Parasitol* **38**, 1651-1662 (2008). https://doi.org:10.1016/j.ijpara.2008.05.012

1032 **FIGURE LEGENDS**

1033 **Figure 1**. ***HsNR4A3* is highly upregulated during *Plasmodium* exoerythrocytic infection. a.**
1034 Schematic representation for culture, sorting by FACs, dual RNA Seq and confocal microscopy
1035 strategies, **b.** Volcano plot of differently expressed genes, gene-expression pattern vs *p* value, with
1036 the position of *HsMUC13, HsCGA, HsSLC22A8, HsMALAT1, HsRASSF9, HsSDHA,*
1037 *HsSLC25A27, HsNEAT1, HsTAS2R4*, *HsCXCL2,* and *HsNR4A3* genes indicated at 24 and 48hpi.
1038 **c.** RT-qPCR of *HsMUC13, HsCGA, HsSLC22A8, HsMALAT1, HsRASSF9, HsSDHA,*
1039 *HsSLC25A27, HsNEAT1, HsTAS2R4,* and *HsNR4A3* at 48hpi in the indicated cell lines. *HsSDHA*
1040 was used as a control. Relative quantitation of the indicated host transcripts calculated using ΔΔCT
1041 method, in the indicated hepatocyte cell types (data presented as mean ± s.e.m, *n*=3 with individual
1042 biological replicates overlaid, * = *p* value 0.05, ** = *p* value 0.001, *** = *p* value 0.0001, **** =
1043 *p* value <0.0001. *p* values determined by two-tailed *t* test). Data from LaMonte et al.[17].

1044

1045 Edited version—please check very carefully, especially for colors, which don't make sense.

1046 **Figure 2. Immunofluorescence micrographs of *Plasmodium*-infected cells using antibodies to**
1047 **HsNR4A3, HsCGA, HsGOLGA8A, and HsMUC13.** Shown are representative confocal
1048 microscopy images of: **a.** HC-04 liver cells infected with *P. berghei* parasites 48hpi; **b.** primary
1049 hepatocytes infected with *P. falciparum* parasites 120hpi; **c.** HC-04 liver cells infected with *P.*
1050 *vivax* schizonts 120hpi; and **d.** HC-04 liver cells infected with *P. vivax* hypnozoites (white filled
1051 arrowheads) 120hpi. Parasites were visualized with a goat-α-PbUIS4 (#LS-C204260) (panels a,
1052 b, a1, a2, a3) or a mouse-α-PvUIS4 (panel c, d, d1) primary and bovine-α-goat
1053 (#805297008, Rhodamine Red (panels a, b)) or donkey-α-mouse (#715297003, Rhodamine
1054 Red (panels c, d)) secondary antibodies. Membranes were stained with CellMask deep red
1055 (magenta) and nuclei were labeled with DAPI (blue). Primary and secondary antibody
1056 combinations for human proteins (green) were as follows: mouse α-HsNR4A3 (HsNR4A3-Ab1)
1057 and donkey α-mouse (#A32766, Alexa Fluor 488 - Green); rabbit α-HsCGA (HsCGA-Ab1), rabbit
1058 α-HsGOLGA8A (HsGOLGA8A-Ab1), or rabbit α-HsMUC13 (HsMUC13-Ab1) primary
1059 antibodies and goat-α-rabbit (#111545046, Alexa Fluor 488 – Green) secondary antibodies. For a-
1060 d, scale bars are 10μm. In the DAPI (blue) panel, the infected (I) and uninfected (UI) cells are

1061 labeled. Parasite nuclei (PN) and the host nucleus (HN) are shown (white filled arrows). Lower
1062 panels show zooms and panoramic fields for NR4A3 stained as described above for *P. berghei*
1063 infected cells (a1, a2, a3) or *P. vivax* infected cells (d1). Golgi in uninfected HC-04 cells are show
1064 (Golgi-UI, white filled arrows on panel a). All images were taken with a 63× oil objective.

1065 **Figure 3: Time-dependent relocalization of HsNR4A3 protein in HC-04 cells infected with *P.***
1066 ***berghei* parasites a.** Micrographs show HC-04 cells uninfected (0h), and infected with *P. berghei*
1067 EEFs at different times (6, 12, 18, 24, 48, and 72hpi). Human host protein was labeled using a α-
1068 HsNR4A3 (HsNR4A3-Ab1) and visualized with a donkey α-mouse secondary antibody
1069 (#A32766, Alexa Fluor 488 – Green); *P. berghei* parasites were labeled using α-PbUIS4 (#LS-
1070 204260) antibody and visualized with a bovine α-goat secondary antibody (#805297008,
1071 Rhodamine red). CellMask deep red was used for plasma membranes (magenta). Nuclei were
1072 labeled with DAPI (blue). Merged images between HsNR4A3, PbUIS4, DAPI, and Cell
1073 Membrane are shown. Scale bars 10μm; 63× oil objective. Two micrographs show HC-04 cells
1074 infected with *P. berghei* parasites (48h) and labeled with a single primary antibody (α-PbUIS4 or
1075 HsNR4A3-Ab1). In the DAPI (nuclei) panels, the infected (I) and non-infected (UI) cells are
1076 labeled. Parasite nuclei (PN) and the host nucleus (HN) are also shown (pointed with white filled
1077 arrows). **b.** Schematic representation of HsNR4A3 relocalization during *Plasmodium*
1078 exoerythrocytic infection in infected liver cells.

1079 **Figure 4. U-ExM of Huh7.5.1 cells infected with *P. berghei* parasites shows HsNR4A3 protein**
1080 **at the PVM.** Five representative micrographs show Huh7.5.1 cells 48hpi with *P. berghei* parasites
1081 prepared for U-ExM (see Methods), stained with a nuclear stain (Sytox Deep Red in cyan), α-
1082 PbUIS4 (in magenta), HsNR4A3-Ab1 (in yellow) and a protein stain (NHS-ester, in grayscale)
1083 and visualized using Airyscan 2 microscopy. Yellow arrows indicate concentration of HsNR4A3
1084 in pockets associated with the PVM. Scale bars as labelled in each image, solid bar = XY scale
1085 and all images are Z-projections with a combined depth of slices of 0.39 μm.

1086 **Figure 5. Relocation of HsCXCL2 protein in HC-04 cells infected with *P. berghei* parasites**
1087 **in different periods (2, 24, and 48hpi). a.** Representative immunofluorescence confocal
1088 micrographs show HC-04 cells infected with *P. berghei* parasites, treated with LPS (1μg/ml) using
1089 indicated time. Cells were labeled using rabbit-α-HsCXCL2 (HsCXCL2-Ab1) antibody and

1090 visualized with a donkey α-rabbit secondary antibody (#711296152, Rhodamine red); CellMask
1091 deep red was used for plasma membranes (Cell Membrane - magenta). *P. berghei* parasites were
1092 labeled using a goat-α-PbUIS4 (#LS-204260) antibody and visualized with a donkey-α-goat
1093 secondary antibody (#705546147, Alexa Fluor 488 - Green). Nuclei were labeled with DAPI (blue)
1094 with the infected (I) and non-infected (UI) cells with parasite nuclei (PN) and the host nucleus
1095 (HN) also shown (white filled arrows). Scale bars 10μm; 63× oil objective. Single primary
1096 antibody labeling (α-PbUIS4 or HsCXCL2-Ab1) in infected and uninfected cells without (w/o)
1097 and with (w/) LPS treatment are shown. Scale bars 10μm; 63× oil objective. **b.** Pearson's
1098 correlation coefficient (PCC) between α-PvUIS4 and HsCXCL2-Ab1 staining. Images were
1099 analyzed with Volocity 3D/4D Rendering Software, and PCC was calculated for identified objects.
1100 Each point represents one infected cell from one of three biological replicates. Data were analyzed
1101 with a two-tailed *t* test, * = $p < 0.0112$, **** = $p < 0.0001$.

1102

1103

1104

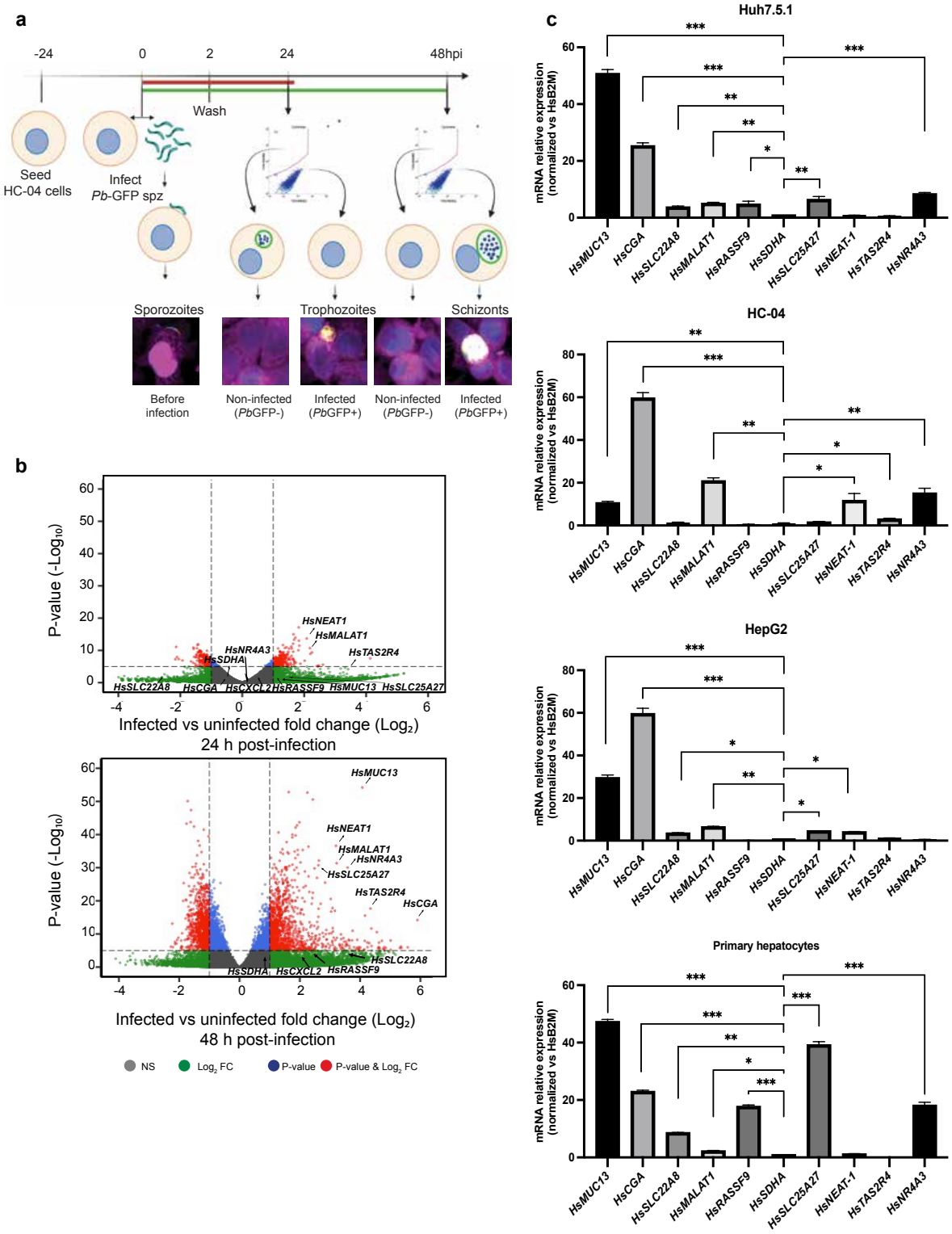
a
-24
0
2
24
48hpi
Wash
Seed
HC-04 cells
Infect
Pb-GFP spz
Sporozoites
Trophozoites
Schizonts
Before infection
Non-infected (PbGFP-)
Infected (PbGFP+)
Non-infected (PbGFP-)
Infected (PbGFP+)
b
P-value (-Log10)
Infected vs uninfected fold change (Log2)
24 h post-infection
HsNEAT1
HsMALAT1
HsNR4A3
HsSDHA
HsTAS2R4
HsSLC22A8
HsCGA
HsCXCL2
HsRASSF9
HsMUC13
HsSLC25A27
48 h post-infection
NS
Log2 FC
P-value
P-value & Log2 FC
c
Huh7.5.1
HC-04
HepG2
Primary hepatocytes
mRNA relative expression (normalized vs HsB2M)
HsMUC13
HsCGA
HsSLC22A8
HsMALAT1
HsRASSF9
HsSDHA
HsSLC25A27
HsNEAT-1
HsTAS2R4
HsNR4A3

Figure 1

1129

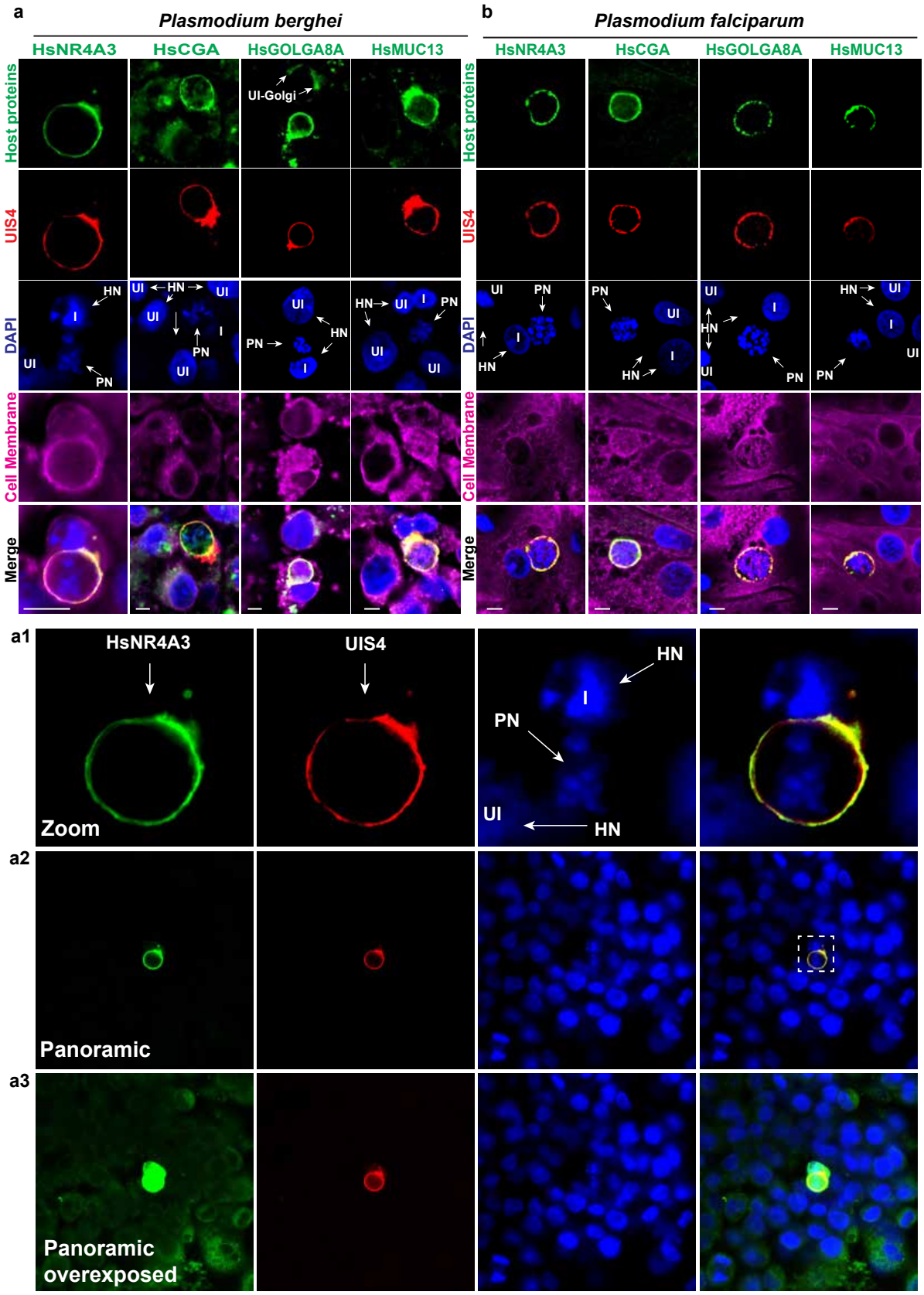
a
Plasmodium berghei
b
Plasmodium falciparum
HsNR4A3
HsCGA
HsGOLGA8A
HsMUC13
Host proteins
UIS4
DAPI
Cell Membrane
Merge
UI-Golgi
HN
I
UI
PN
a1
a2
a3
Zoom
Panoramic
Panoramic overexposed

1130

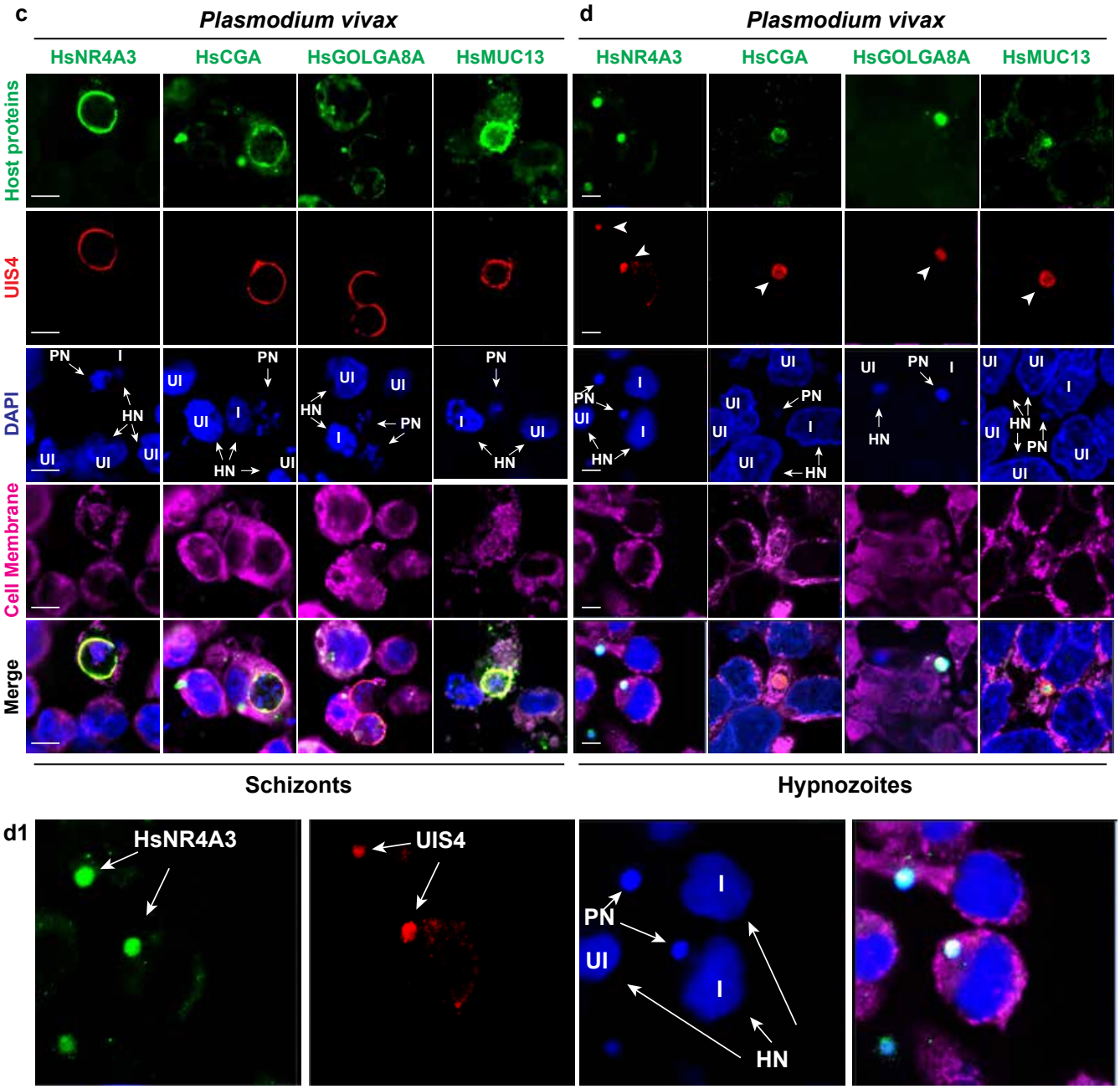

1131

1132

1133 Figure 2

1134

1135

1136

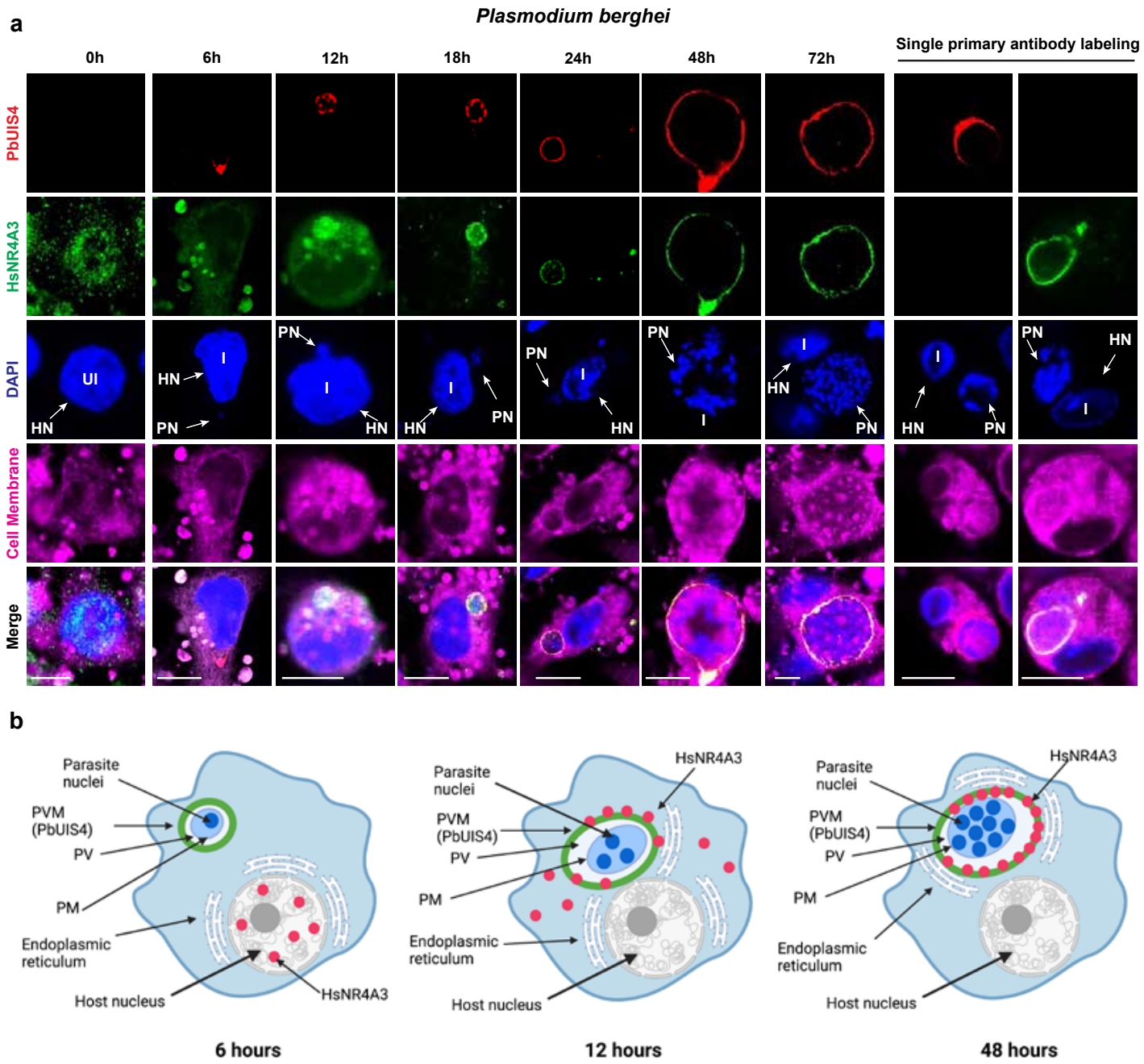
a
Plasmodium berghei
0h
6h
12h
18h
24h
48h
72h
Single primary antibody labeling
PbUIS4
HsNR4A3
DAPI
Cell Membrane
Merge
UI
HN
PN
I
b
Parasite nuclei
PVM (PbUIS4)
PV
PM
Endoplasmic reticulum
Host nucleus
HsNR4A3
6 hours
12 hours
48 hours

Figure 3

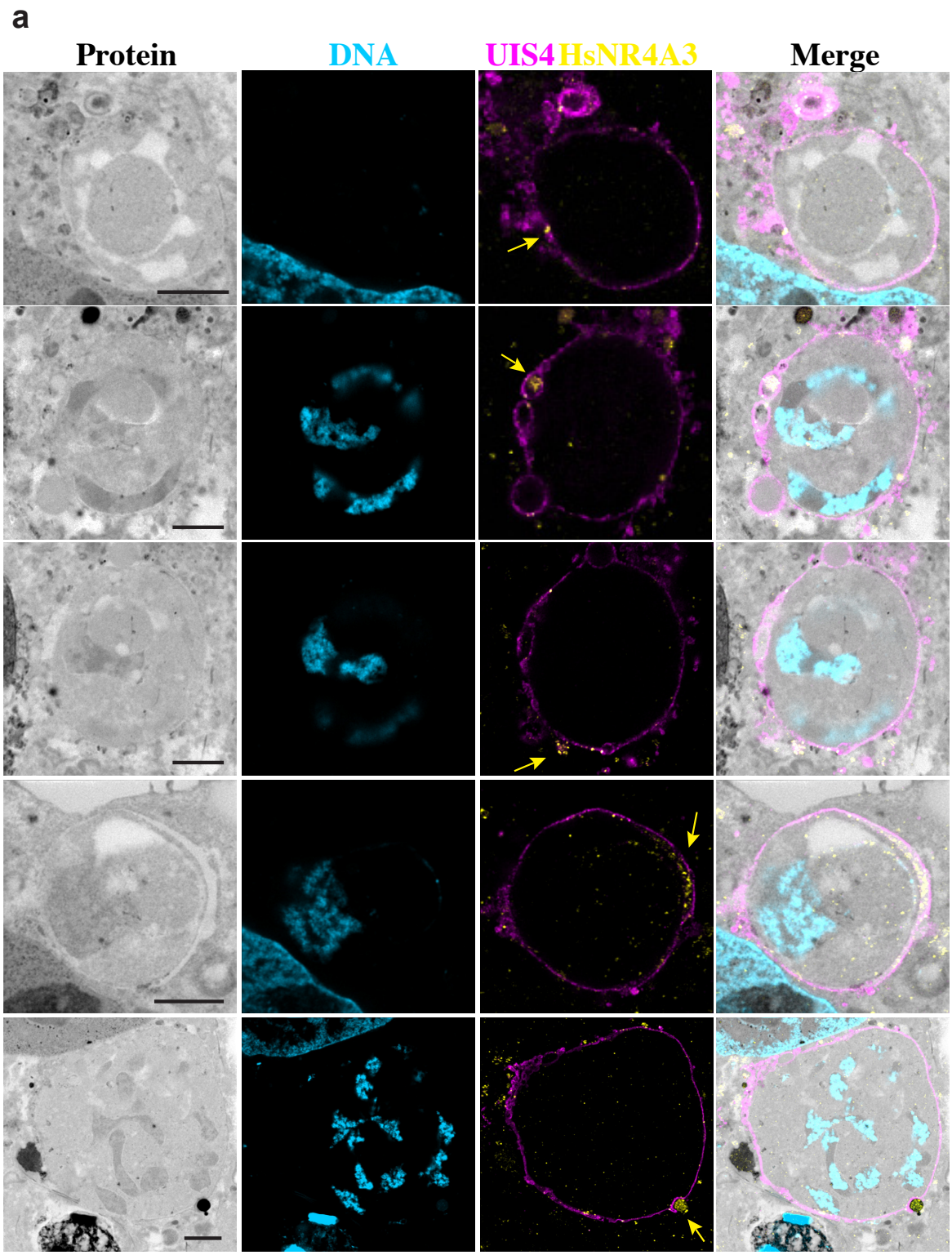

Figure 4

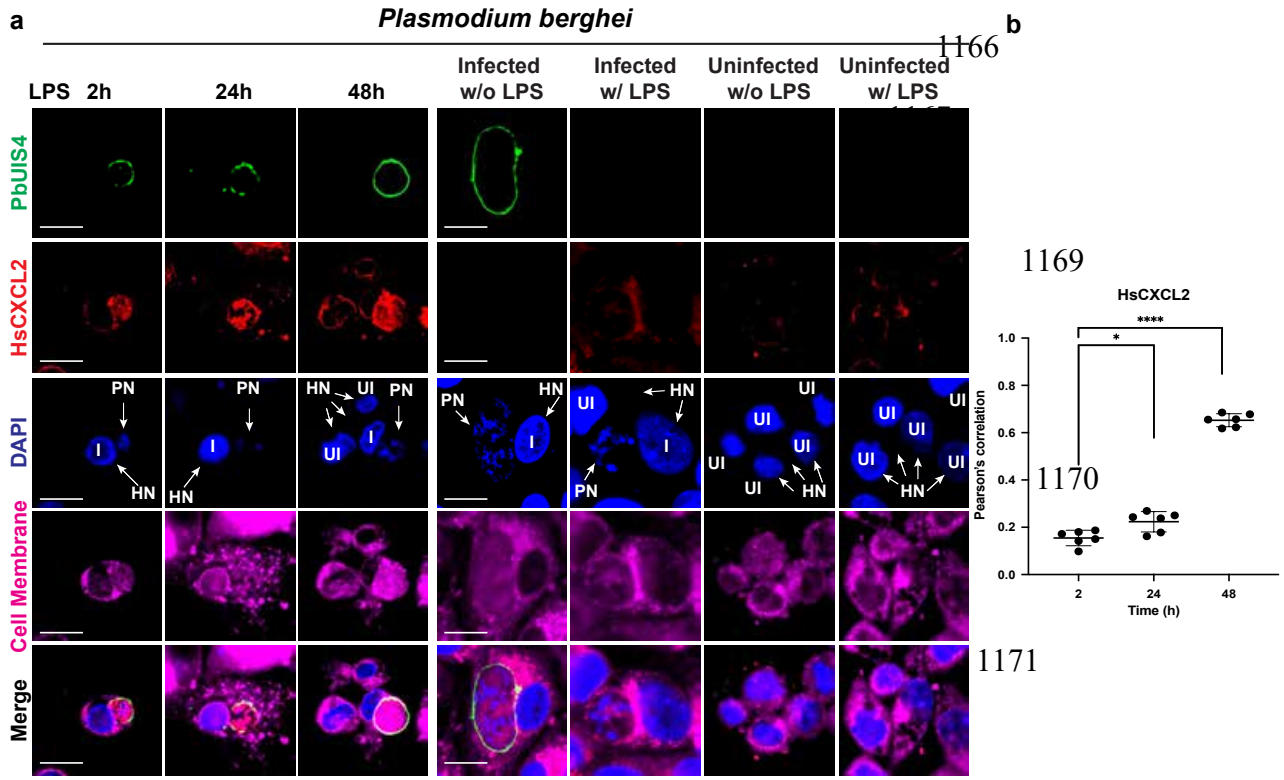
a
Plasmodium berghei
b
LPS 2h
24h
48h
Infected w/o LPS
Infected w/ LPS
Uninfected w/o LPS
Uninfected w/ LPS
PbUIS4
HsCXCL2
DAPI
Cell Membrane
Merge
PN
HN
I
UI
HsCXCL2
****
*
Pearson's correlation
Time (h)
2
24
48
0.0
0.2
0.4
0.6
0.8
1.0

Figure 5